

THE COSMIC RATE, LUMINOSITY FUNCTION AND INTRINSIC CORRELATIONS OF LONG GRBS

NATHANIEL R. BUTLER¹, JOSHUA S. BLOOM^{2,3}, & DOVI POZNANSKI^{2,4}

Submitted to ApJ

ABSTRACT

We calculate durations and spectral parameters for 207 Swift bursts detected by the BAT instrument from April 2007 to August 2009, including 67 events with measured redshifts. This is the first supplement to our catalog of 425 Swift GRBs (147 with redshifts) starting from GRB 041220. This complete and extensive data set, analyzed with a unified methodology, allows us to conduct an accurate census of intrinsic GRB energetics, hardnesses, durations, and redshifts. The GRB world model we derive reproduces well the observables from both Swift and pre-Swift satellites. Comparing to the cosmic star formation rate, we estimate that only about 0.1% of massive stars explode as bright GRBs. There is strong evidence for evolution in the Swift population at intermediate and high- z , and we can rule out (at the 5-sigma level) that this is due to evolution in the luminosity function of GRBs. Instead, the Swift sample suggests a modest propensity for low-metallicity, evidenced by an increase in the rate density with redshift. Treating the multivariate data and selection effects rigorously, we find a real, intrinsic correlation between E_{iso} and E_{pk} (and possibly also $T_{r45,z}$); however, the correlation *is not* a narrow log-log relation and its observed appearance is strongly detector-dependent. We also estimate the high- z rate (3 – 9% of GRBs at z beyond 5) and discuss the extent of a large missing population of low- $E_{\text{pk,obs}}$ XRFs as well as a potentially large missing population of short-duration GRBs that will be probed by EXIST.

Subject headings: gamma rays: bursts — methods: statistical — Gamma-rays: general

1. INTRODUCTION

The *Swift* satellite (Gehrels et al. 2004) has transformed the study of Gamma-ray Bursts (GRBs) and their afterglows. Our knowledge of the early X-ray afterglows has increased tremendously due to the dramatic success of the X-ray Telescope (XRT; Burrows et al. 2005). However, our understanding of the prompt emission properties has lagged. This is due in part to the narrow energy bandpass of the Burst Alert Telescope (BAT; Barthelmy et al. 2005), which precludes direct measurement of the broad GRB spectra and tends to weaken any inferences about the νF_{ν} spectral peak energy $E_{\text{pk,obs}}$ and the bolometric GRB fluence.

In the first installment of our “Complete BAT Catalog of Swift GRBs and Spectra” (Butler et al. 2007, hereafter Paper I), we treat these limitations of the BAT in a statistically rigorous fashion and study tantalizing pre-Swift correlations between the host-frame characteristics of GRBs (e.g., Lloyd, Petrosian, & Malozzi 2000; Fenimore & Ramirez-Ruiz 2000; Norris, Marani, & Bonnell 2000; Schaeffer 2003; Amati et al. 2002; Lamb et al. 2004; Ghirlanda, Ghisellini, & Lazzati 2004; Firmani et al. 2006). A number of these potential log-log relations appear dramatically different in the Swift-era sample, with a broader scatter, and a shift in normalization toward the detector threshold. From this, we concluded that the origin of these correlations was tied more closely to the detection process than to the intrinsic physics of

GRBs.

We present here fits to the lightcurves and spectra of additional Swift GRBs detected between April 17, 2007 and August 13, 2009, nearly doubling the overall sample. As summarized in Paper I and below, our analysis is extremely uniform (nearly fully-automated), with well-defined survey flux limits, and our fits allow for detailed propagation of errors. These features are critical to the estimate of GRB rates, the focus of the current work. Our primary goal is to uncover, with realistic estimates of uncertainty, the intrinsic GRB production rate as a function of redshift $\dot{\rho}(z)$. To measure this quantity, it is necessary to model the GRB luminosity function $\phi(L)$ allowing for possible intrinsic and detection-based correlations.

We derive a model that describes both Swift and pre-Swift rates well as a function of hardness, duration, flux, and redshift (Section 2). As we discuss in Section 2.6 below, we find a highly significant, intrinsic correlation between E_{iso} and E_{pk} ; however, the observed correlation has large scatter and is strongly instrument-dependent. Figure 1 shows how the overall number of events observed by Swift — and not just the correlation between observed quantities — requires us to build temporal and spectral dependences into modelling the luminosity function.

In the next section, we summarize the utility and historical background behind making a plot like Figure 1. We then discuss in Section 2.6 the models that successfully recreate the curves in Figure 1 and also the implications for the GRB luminosity function (Section 3.1) and comoving rate density (Section 3.2). In Section 3.4 we make self-consistent predictions for the expected observed redshift distribution for all Swift GRBs — including the 60% fraction of Swift GRBs for which a spectroscopic z has not been measured — and also for the

¹ Einstein Fellow, Astronomy Department, University of California, Berkeley, CA, 94720-7450, USA

² Astronomy Department, University of California, Berkeley, CA, 94720-7450, USA

³ Sloan Research Fellow

⁴ Lawrence Berkeley National Laboratory, 1 Cyclotron Road, Berkeley, CA 94720, USA

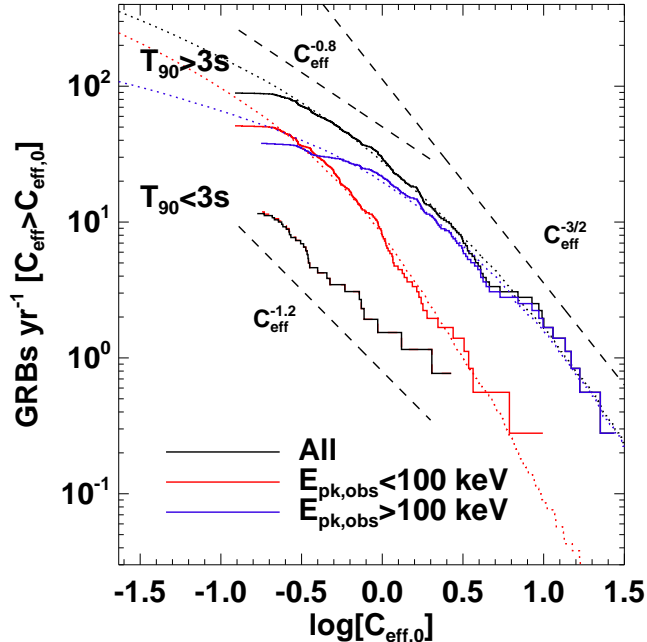


FIG. 1.— Strong spectral and temporal dependence in the number of GRBs with effective count rate C_{eff} (Section 2.2) above a given value (i.e., the Swift “logN–logS” curve; see Section 1.1). We plot here long duration ($T_{90} > 3$ s) GRBs with hardness above and below the median Swift $E_{\text{pk,obs}} = 100$ keV and also short duration ($T_{90} < 3$ s) GRBs. The rate of long-duration hard GRBs is turning over at low flux levels, while the rate of long-duration soft GRBs rises more strongly. This is a gradual effect in $E_{\text{pk,obs}}$. Although the logN–logS slope for long-duration GRBs does not appear to be duration dependent, the Swift short-duration GRB population is strongly rising in number to low flux levels, showing no significant sign of a turn-over. The curves expected without a cutoff — derived in Section 2.6 — due to the detector are plotted as dotted lines. The dashed red curve (barely visible) at the left of the short-duration curve accounts for the detector threshold following the non-parametric prescription of Petrosian & Lee (1996).

planned and more-sensitive EXIST experiment. We expect EXIST to thrive with respect to the detection of both short and long duration GRBs at high redshift.

1.1. Prior Rate and Luminosity Function Estimates

There is a rich literature describing optimal ways of counting GRBs to determine their distance and intrinsic flux. In the pre-afterglow era, counting focused on the observed flux distributions. The number of events N with observed flux greater than S — the so called “logN–logS” curve — showed early evidence (over many decades in S) for slope $S^{-3/2}$ expected for a homogeneous, isotropic, and static source population in a Euclidean universe (HISE; e.g., Hurley 1991; Higdon & Schmidt 1990). A powerful statistic for examining the source counts is $V/V_{\text{max}} = (C/C_{\text{min}})^{-3/2}$ (Schmidt 1968), a measure of the volume probed by a source detected with C counts relative to a possible minimum number of observable counts C_{min} . The expectation is that $\langle V/V_{\text{max}} \rangle = 0.5$ for HISE. The BATSE experiment provided the first strong evidence from a single experi-

ment (Meegan et al. 1992) — a deficit of low S GRBs and $\langle V/V_{\text{max}} \rangle < 0.5$ — for a departure from homogeneity, while the spatial counts showed clearly an isotropic population. To study whether these modest departures imply that GRBs are very local (a Galactic halo population) or cosmological required examination beyond the first moment $\langle V/V_{\text{max}} \rangle$ in the V (or C) distribution (e.g., Band 1992; Hartmann & The 1993; Petrosian 1993).

The first GRB redshifts (e.g., Metzger et al. 1997) defined a cosmological origin and a vast energy release. Connecting the small number of GRBs with z to the large population of GRBs without z required, in general, careful modelling of and strong assumptions for the intrinsic luminosity and number density distributions in order to reproduce the observed flux data (e.g., Piran 1992, 1999; Cohen & Piran 1995; Fenimore & Bloom 1995; Loredano & Wasserman 1995, 1998; Horack & Hakkila 1997; Schmidt 1999, 2001; Sethi & Bhargavi 2001; Guetta et al. 2005). Exceptions to the parametric approach were studies utilizing luminosity criteria (i.e., possible correlations of observables with luminosity) to derive “pseudo-redshifts” for the full GRB sample (e.g., Norris et al. 2000; Fenimore & Ramirez-Ruiz 2000; Schaefer et al. 2001; Lloyd-Ronning et al. 2002; Murakami et al. 2003; Yonetoku et al. 2004; Firmani et al. 2004; Kocevski & Liang 2006; Schmidt 2009). These studies generally found a rising GRB rate to $z \lesssim 2$, similar to the cosmic star formation rate (e.g., Madau et al. 1996), but potentially continuing to remain flat or even rising to $z \sim 12$.

Notably, some of these works (e.g., Lloyd-Ronning et al. 2002; Yonetoku et al. 2004), using hazard statistics (Lynden-Bell 1971; Efron & Petrosian 1992; Petrosian 1993; Maloney & Petrosian 1999), also found evidence for potential strong luminosity evolution, parameterized as $L \propto (1+z)^a$, with a in the range 1.5–2.5. The luminosity function itself appears to generally be characterized well as broken powerlaw, with a break at $L \sim 10^{51-52}$ erg s $^{-1}$ and a flat or slowly rising slope to low-energies, strongly dependent upon the instrumental detection model.

The connection between GRBs and the deaths of massive stars (now firmly established, e.g., Stanek et al. (2003); Hjorth et al. (2003); see Woosley & Bloom (2006) for a review) sped progress by motivating an assumption that the GRB rate follows star formation (e.g., Wijers et al. 1998; Lamb & Reichart 2000; Porciani & Madau 2001; Choudhury & Srianand 2002; Bloom 2003; Gorosabel et al. 2004; Natarajan et al. 2005). Very recently, thanks to Swift and the impressive efforts of ground-based observers, a growing sample of GRBs with spectroscopic redshifts has allowed for direct tabulation of GRB intrinsic luminosities (e.g., Kocevski & Butler 2008) and redshifts (e.g., Jakobsson et al. 2005, 2006).

The large number of redshifts has also enabled a detailed comparison of the intrinsic GRB rate to the cosmic star formation rate (SFR, e.g., Daigne et al. 2006; Salvaterra & Chincarini 2007; Kistler et al. 2008, 2009; Salvaterra et al. 2009a,b). Perhaps the most intriguing, shared feature of these studies is a strong indication of evolution in the GRB population. Above $z \approx 2$ and possibly extending to $z \approx 8$, the Swift GRB rate is increasing far faster than star formation (e.g., Kistler et al. 2008, 2009), and it is not clear to what extent this is due to GRBs in the early universe being bright (i.e., luminos-

ity evolution, preferred by Salvaterra & Chincarini 2007; Salvaterra et al. 2009a,b; Petrosian et al. 2009) or to an increase in the overall number of GRBs at intermediate and high- z relative to the SFR.

As we discuss below in Section 3.2, rigorous treatment of the largest available Swift dataset (Section 2) allows for a firm conclusion in favor of rate evolution and not luminosity evolution, and we suggest plausible explanations. To draw this conclusion and to study GRB rates as a function of intrinsic hardness, flux, and duration (Sections 2.6 & 3.1) as well as z , we require a detailed model for the Swift satellite detection limit (Section 2.1).

2. DATA REDUCTION AND FITS

Our automated pipeline at the University of California, Berkeley is used to download the *Swift* data in near real time from the *Swift* Archive⁵ and quicklook site. We use the calibration files from the 2008-12-17 BAT database release. We establish the energy scale and mask weighting for the BAT event mode data by running the `bateconvert` and `batmaskwtevt` tasks from the HEASoft 6.6.1 software release⁶. Spectra and light curves are extracted with the `batbinevt` task, and response matrices are produced by running `batdrngen`. We apply the systematic error corrections to the low-energy BAT spectral data as suggested by the BAT Digest website⁷ (see, also Sakamoto et al. 2008), and fit the data in the 15–150 keV band using ISIS⁸. The spectral normalizations are corrected for satellite slews as recommended in BAT Digest. All errors regions reported correspond to the 90% confidence interval. In determining source frame flux values, we assume a cosmology with $h = 0.71$, $\Omega_m = 0.3$, and $\Omega_\Lambda = 0.7$.

The burst duration intervals are determined automatically as described in Paper I and are presented in Table 3 for the current, supplemental sample. Spectral fitting is performed also as described in Paper I, and we present the results in Table 4. Electronic version of the tables — updated in near real time — including additional fit statistics (e.g., fluxes and fluences in various bandpasses) and downloadable reduced data, can be found at the project webpage⁹.

2.1. Sample Selection & Survey Flux Limit

Although Tables 3 & 4 contain data for the full Swift sample, we restrict the rate analysis below to long-duration GRBs ($T_{90} > 3$ s, e.g., Kouveliotou et al. 1993) with signal-to-noise ratios $S/N > 10$. The separation of short and long duration GRBs is motivated by the potential that the duration classes map to separate source populations (e.g., Zhang et al. 2008; Nysewander et al. 2009; Levesque et al. 2009, and references therein), also suggested by the sharp logN–logS slope variation (Figure 1) for short GRBs relative to long GRBs. We exclude 3 GRBs (051109B, 060218, and 060614) at $z < 0.2$ due to data quality issues (uncertain redshift, missing data, possible short duration, respectively; see Paper I). We note that the $\approx 6\%$ of BAT GRBs detected in ground analyses are not included in this catalog.

⁵ <ftp://legacy.gsfc.nasa.gov/swift/data>

⁶ <http://swift.gsfc.nasa.gov/docs/software/lheasoft/download.html>

⁷ http://swift.gsfc.nasa.gov/docs/swift/analysis/bat_digest.html

⁸ <http://space.mit.edu/CXC/ISIS>

⁹ <http://astro.berkeley.edu/~nat/swift>

Central to our analysis is a burst-by-burst estimate of the minimum detectable count rate. As discussed in Paper I, an a-posterior estimate of the optimal imaging S/N for every GRB detected by BAT can be obtained by generating the demasked light curve using the XRT position for the GRB. The temporal region which maximizes the S/N can be found, and this maximal S/N (see Table 1) bounds that achievable by the BAT trigger software. The maximal S/N can be used to infer the minimum detectable counts C_{\min} relative to the observed number of counts C : $C_{\min} = C(10/[S/N])$ (10σ detection limit). This is a valid approximation only in the background-dominated noise regime, and there is a modest $\approx 10\%$ correction in the case of a handful of the very brightest Swift GRBs.

This C_{\min} estimate effectively treats the BAT trigger software as perfect, always able to find the optimal S/N region. This approximation should break down in the limit of low S/N , which is why we have chosen 10σ (as opposed to, e.g., 5σ). The observed C/C_{\min} distribution turns over below 10σ , justifying this choice.

As discussed in detail in Paper I, the photon fluence over root duration correlates strongly with our S/N measure, indicating that the BAT instrument sensitivity is best characterized in such units (see, also, Sakamoto et al. 2007). We can define an effective count rate $C_{\text{eff}} = C\sqrt{f_p/T_{r45}}$, where f_p is the partial coding fraction resulting from the position of the GRB in the BAT field-of-view, and T_{r45} is the high-signal time duration of Reichart et al. (2001). This duration measure should provide a good link between the time-integrated flux and the flux — while the GRB is bright — relevant for triggering. The quantity $C_{\text{eff}}/[S/N]$ clusters tightly with a scatter $\lesssim 0.1$ dex, indicating an effective BAT threshold count rate of $C_{\text{eff},\min} = 0.24 \pm 0.05$ cts/s^{0.5}/fully-coded-detector (10σ). We interpret the uncertainty in this number as the uncertainty in our ability to measure the true threshold count rate given our estimate of that rate.

It is a very poor approximation, alternatively, to model Swift as a peak photon flux detector like BATSE. Swift GRBs with $S/N < 10$ have peak photon fluxes in the 15–150 keV band ranging from 0.1 to 1 ph cm⁻² s⁻¹. It would be necessary to discard 40% of the full sample (that with peak fluxes below 1 ph cm⁻² s⁻¹) to obtain a clean, flux-limited sample. Worse yet, a 10σ threshold based on 15–150 keV photon fluence over T_{90} duration would need to reject $\gtrsim 60\%$ of the Swift sample to avoid ($p < 0.6$ cm⁻² s⁻¹) GRBs whose numbers are strongly affected by the detection limit. Our approach allows for fitting of 88% of the full sample at 10σ .

2.2. GRB World Model Overview

We wish to derive a model capable of reproducing the observed Swift GRB rate as a function of redshift, flux, hardness, and duration. As discussed above, these quantities are known to — or have been argued to — exhibit strong correlations. Therefore, all must be considered in deriving reliable rates. Additional quantities (e.g., to describe GRB beaming) may be important but are not readily accessible in order to be grafted onto the present catalog. Our formalism rigorously accounts for measurement errors and for correlations present in the data.

We characterize the GRB rate as a product of terms

involving the redshift z of the bursts, the isotropic equivalent energy release ($1\text{--}10^4$ keV) E_{iso} , the duration T_{r45} , and also the hardness $E_{\text{pk,obs}}$ of the bursts. To describe correlations among these quantities, it is sufficiently general (see Appendix) to define an effective bolometric luminosity L :

$$L = \frac{E_{\text{iso}}}{(1+z)^{\alpha_z}} \left(\frac{10^{2.5}\text{keV}}{E_{\text{pk}}} \right)^{\alpha_E} \left(\frac{10^{0.6}\text{s}}{T_{r45,z}} \right)^{\alpha_T}. \quad (1)$$

We assume a smoothly broken powerlaw for the luminosity function:

$$\phi_L = \frac{dN}{d \log L} = \begin{cases} (L/L_{\text{cut}})^{\alpha_L} & L < L_{\text{cut}} \\ (L/L_{\text{cut}})^{\beta_L} & L \geq L_{\text{cut}}. \end{cases} \quad (2)$$

We make this function smooth by convolving it with a Gaussian in $\log(L)$ of width σ_L , resulting in $\phi(L) \rightarrow \tilde{\phi}(L|\sigma_L)$. In the case of no luminosity correlations (α 's all zero), $\tilde{\phi}$ is the distribution for E_{iso} .

The true, detector-independent differential rate (per z , per $\log E_{\text{iso}}$, $\log E_{\text{pk}}$, $\log T_{r45,z}$) can then be written:

$$r_{\text{true}} = \tilde{\phi}(L) P_E(E_{\text{pk}}) P_T(T_{r45,z}) \frac{r_0 \dot{\rho}(z) dV/dz}{(1+z)}, \quad (3)$$

where $P_E(E_{\text{pk}})$ is the intrinsic E_{pk} distribution, $P_T(T_{r45,z})$ is the intrinsic distribution in $T_{r45,z}$, and $\dot{\rho}(z)$ is the comoving GRB rate density. The universal volume is V , and the factor $(1+z)$ accounts for cosmic time dilation. The normalization $r_0 \propto dt d\Omega / \langle f_{\text{beam}} \rangle$ includes the survey duration, solid angle $d\Omega \approx 1.4$ sr, and the effects of GRB beaming. Functional forms for $P_E(E_{\text{pk}})$, $P_T(T_{r45,z})$, and $\dot{\rho}(z)$ are described below.

For a given GRB, the expected number of BAT counts C (Section 2) in the trigger time window depends on L , E_{pk} , $T_{r45,z}$, and z . The GRB will be detected when $C > C_{\text{min}}$, where C_{min} depends approximately on T_{r45} alone, yielding the observed GRB rate:

$$r_{\text{obs}} = \Theta(C - C_{\text{min}}) r_{\text{true}}. \quad (4)$$

We fit this multivariate model (Section 2.6) by evaluating and maximizing r_{obs} at each observed data point (see Appendix for more details).

2.3. The GRB Rate Density

Based on the shape of the cosmic star formation rate (SFR; Hopkins & Beacom 2006), we assume a broken powerlaw for the comoving GRB rate density:

$$\dot{\rho}(z) = \frac{dN}{dz} \propto \begin{cases} (1+z)^{g_0} & z < 0.97 \\ (1+z)^{g_1} & 0.97 < z < z_1 \\ (1+z)^{g_2} & z > z_1, \end{cases} \quad (5)$$

where the relative normalizations (not written above) are set so that $\dot{\rho}(z)$ is continuous at $z_0 = 0.97$ and z_1 . The SFR has roughly $(g_0, g_1, g_2) = (3.4, -0.3, -8)$ for $z_1 \approx 4.5$ (e.g., Figure 10). For this model to yield acceptable fits to the Swift GRB data (Section 2.6), the parameters g_0 , g_1 , g_2 , and z_1 must be allowed to vary. In fitting this model, we marginalize over the free parameters and derive a best-fit shape that is generally smoother than the input form. Future work can compare star formation models directly to these best-fit curves and error regions without needing to re-fit the Swift data.

2.4. The Intrinsic E_{pk} Distribution

We have tested a variety of functional forms for the intrinsic distribution in $\log[E_{\text{pk}}]$. A normal distribution can fit the observed univariate distribution reasonably well, but it fails to account well for the multivariate distribution in E_{pk} and E_{iso} (Section 2.7). This is because a narrow log-Gaussian cannot generate a large enough dynamic range in E_{pk} to allow for the observed correlation (over many decades in E_{pk}) with E_{iso} . Moreover, the observed E_{pk} distribution is found also to be consistent with intrinsic models formed from the sum of log-Gaussian extending to low E_{pk} . That is, low E_{pk} GRBs have a tendency to go undetected, and the data do not strongly constrain the presence of such populations.

To fit a more general form for the intrinsic $\log[E_{\text{pk}}]$ distribution, we consider the following:

$$P_E = \frac{dN}{d \log E_{\text{pk}}} = \begin{cases} (E_{\text{pk}}/E_{\text{pk},0})^{\beta_E} & E_{\text{pk}} < E_{\text{pk},0} \\ \exp[-\frac{1}{2}(\frac{\log(E_{\text{pk}}/E_{\text{pk},0})}{\sigma_{E_{\text{pk},0}}})^2] & E_{\text{pk}} > E_{\text{pk},0}. \end{cases} \quad (6)$$

This functional form allows for a potential population of low E_{pk} events not readily detected by Swift. We find that the low- E_{pk} powerlaw index β_E tends to be negative, indicating a large number of missing low E_{pk} events. The proposed extent of such a population is not new to this work (e.g., Strohmayer et al. 1998; Lamb et al. 2005; Pelangeon, et al. 2008).

2.5. The Intrinsic $T_{r45,z}$ Distribution

The intrinsic duration distribution $P_T(T_{r45,z})$ appears to be well-modelled as a log-Gaussian with variable mean and width:

$$P_T = \frac{dN}{d \log T_{r45,z}} = \exp[-\frac{1}{2}(\frac{\log(T_{r45,z}/T_{r45,z,0})}{\sigma_{T_{r45,z,0}}})^2]. \quad (7)$$

There is evidence for a modest fraction of missing long-duration events (Figure 2); however additional components to $P_T(T_{r45,z})$ do not appear to be necessary to model this. We note that we use the common transformation between observed duration T_{r45} and intrinsic duration $T_{r45,z} = T_{r45}/(1+z)^{0.6}$ (e.g., Firmani et al. 2006), which accounts for the expected broadening of pulse widths due to spectral evolution observed at softer bandpasses for GRBs at higher z (Fenimore et al. 1995).

2.6. Model Fitting

We fit the rate density model (Equation 4) to the data for 120 Swift GRBs with measured redshift and 205 additional GRBs without measured redshift. We assume uniform priors for all model parameters summarized in Table 1. The fitting is accomplished by maximizing Equation A-5 using Markov Chain Monte Carlo (MCMC) in python with PyMC¹⁰.

We have performed the fitting for two sample divisions: (1) GRBs with redshift only, and (2) GRBs with and without redshift. The best-fit parameters after including GRBs without redshift are closely consistent (1σ level) with those found from considering only the GRBs with redshift. This indicates that Swift GRBs without redshift do not have a strongly different redshift distribution

¹⁰ <http://code.google.com/p/pymc>

as compared to the GRBs with redshifts. In any case, the analysis below does not depend strongly on the inclusion/exclusion of Swift GRBs without measured redshift (see, Section 3.3), apart from the estimate of total expected rates from future experiments (Section 3.4). We will focus on the parameters derived for the full sample, because the redshift-only sample is, in principle, more prone to biases related to obtaining spectroscopic redshifts (Section 3.3).

Figures 2 show the best fit model from Table 1 (including GRBs without redshift) overplotted on the univariate data distributions. The quality of the fits can be judged visually or from a Kolmogorov-Smirnov (KS) test (e.g., Press et al. 1992). In particular, the KS-test null hypothesis probability that the observed redshift distribution is different than the predicted distribution is $P_{KS} = 0.94$, indicating little evidence that the model and data distributions significantly differ. The KS-test, likewise, for the distribution in detected counts C yields $P_{KS} = 0.29$. For the $T_{r45,z}$, L , and $E_{pk,z}$ distributions we find $P_{KS} = 0.77$, $P_{KS} = 0.77$, and $P_{KS} = 0.84$, respectively. We have also performed two-dimensional KS tests (e.g., Press et al. 1992) on the bivariate distributions of E_{iso} with E_{pk} ($P_{KS} = 0.17$; see Figure 6), or $T_{r45,z}$ ($P_{KS} = 0.12$), or z ($P_{KS} = 0.14$), indicating no strong evidence for a poor fit. Considering all of the KS-tests above, the model appears to reproduce the data quite well.

We note that an intrinsic correlation between E_{iso} and E_{pk} is present ($\alpha_E = 1.8 \pm 0.3$) and is highly significant ($\alpha_E > 0$ at 9σ , $-2\Delta \log(\mathcal{L}) = 82.6 \sim \Delta\chi^2$ for one additional degree of freedom). Some of this correlation may be with the variables $T_{r45,z}$ and z ; however, there is little evidence that luminosity evolution ($\alpha_z = 0.0 \pm 0.5$) is present, and the evidence for correlation between E_{iso} and $T_{r45,z}$ ($\alpha_T = 0.40 \pm 0.2$, full sample; $\alpha_T = 0.3 \pm 0.2$ z only) is comparatively weak.

We note that the magnitude (i.e., α_T) of the intrinsic correlation with $T_{r45,z}$ covaries strongly with the center of the intrinsic $T_{rt45,z}$ distribution $\log(T_{rt45,z0})$ (Pearson correlation coefficient $r = -0.74$), which is already displaced toward long $T_{r45,z}$ from the observed distribution (Figure 2). To the extent that we have potentially over-estimated the Swift sensitivity at long durations by assuming that the trigger sensitivity scales indefinitely as $T_{r45}^{-0.5}$, the evidence for an intrinsic correlation between E_{iso} and $T_{r45,z}$ would weaken.

Figure 3 displays the sample correlation matrix. In addition to the covariance just mentioned for α_T and $\log(T_{rt45,z0})$, there are a number of additional parameters which strongly co-vary (Pearson correlation coefficient $r > 0.5$). Covariance is minimized when ignoring the GRBs without measured redshifts: the value of $\log(L_{cut})$ and the strength of possible luminosity evolution α_z exhibit $r = -0.74$, and the center of the intrinsic distributions in E_{pk} correlates with the width of the distribution ($\log(\sigma_{E_{pk,0}})$) with $r = -0.90$.

It is important to note that the parameters describing the rate density do not co-vary strongly with the other parameters. This is not true when the sample without redshift is included in the analysis. In that case, the slope of $\dot{\rho}$ between $z = 0.97$ and $z \approx 4$ covaries with $\log(L_{cut})$ ($r = 0.54$) and with the evolution index α_z ($r = -0.63$). Finally, the $E_{iso} - E_{pk}$ correlation index α_E

anti-correlates strongly with the parameter β_E describing the rate of missing low- E_{pk} GRBs, particularly in the case where the GRBs without redshifts are included ($r = -0.80$).

TABLE 1
BEST-FIT GRB WORLD MODELS

parameter	value (all GRBs)	value (w/ z only)
Luminosity Func.		
α_L	-0.22 (-0.18,+0.31)	-0.27 \pm 0.19
b_L	-2.89 (-2.05,+1.06)	-3.46 \pm 1.53
$\log[L_{cut}]$	52.74 \pm 0.43	52.95 \pm 0.31
$\log[\sigma_L]$	-1.57 \pm 1.16	-1.78 \pm 1.12
Rate Density		
g_0	3.14 \pm 0.71	3.35 \pm 0.74
g_1	1.36 \pm 0.58	1.32 \pm 0.58
g_2	-2.92 (-2.36,+1.58)	-2.51 (-2.25,+1.60)
z_1	4.00 \pm 0.38	3.98 \pm 0.38
E_{iso} Correlations		
α_E (E_{pk})	1.77 \pm 0.28	1.59 (-0.24,+0.32)
α_T ($T_{r45,z}$)	0.40 \pm 0.15	0.27 \pm 0.22
α_z (z)	0.05 \pm 0.49	-0.12 \pm 0.45
E_{pk} dist.		
$\log[E_{pk,0}]$	2.60 (-0.42,+0.27)	2.60 (-0.51,+0.33)
β_E	-0.51 \pm 0.47	-0.29 (-0.45,+0.69)
$\log[\sigma_{E_{pk,0}}]$	-0.65 \pm 0.26	-0.57 (-0.34,+0.25)
$T_{r45,z}$ dist.		
$\log[T_{r45,z0}]$	0.63 \pm 0.07	0.68 \pm 0.11
$\log[\sigma_{T_{r45,z0}}]$	-0.33 \pm 0.03	-0.32 \pm 0.05
Threshold		
$\log[C_{eff,min}]$	-0.59 \pm 0.01	-0.59 \pm 0.02

2.7. Pre-Swift Distributions

To gauge the validity of the model fit above to the Swift sample, we can compare the model predictions to data obtained from pre-Swift experiments. We do this here for the hardness and flux distributions. Studies of the duration distributions (e.g., Levesque et al. 2009) also appear to demonstrate consistency.

Although it was not a requirement of our fits, a significant number of low- $E_{pk,obs}$ events — many of which are not detected by Swift — are required to account for the large relative number of X-ray Flashes (XRFs; Heise et al. 2001) detected by HETE-2 (e.g., Sakamoto et al. 2005) and *Ginga* (e.g., Strohmayer et al. 1998). This has been discussed elsewhere, for example, by Lamb et al. (2005). Figure 4 shows the expected distributions in $E_{pk,obs}$ for HETE-2 and BATSE.

The BATSE LAD trigger efficiency relative to Swift BAT is taken from (Band 2006). To reproduce the relative fraction of bright GRBs in Kaneko et al. (2006), we adopt a factor 8 sensitivity decrease relative to the full BATSE sample. From a KS-test ($P_{KS} = 0.32$), the predicted and observed distributions do not differ strongly.

The sensitivity curve for HETE-2 is taken to be the WXM sensitivity curve of Band (2003), with the modification to account for $\Delta t > 1s$ triggers from Lamb et

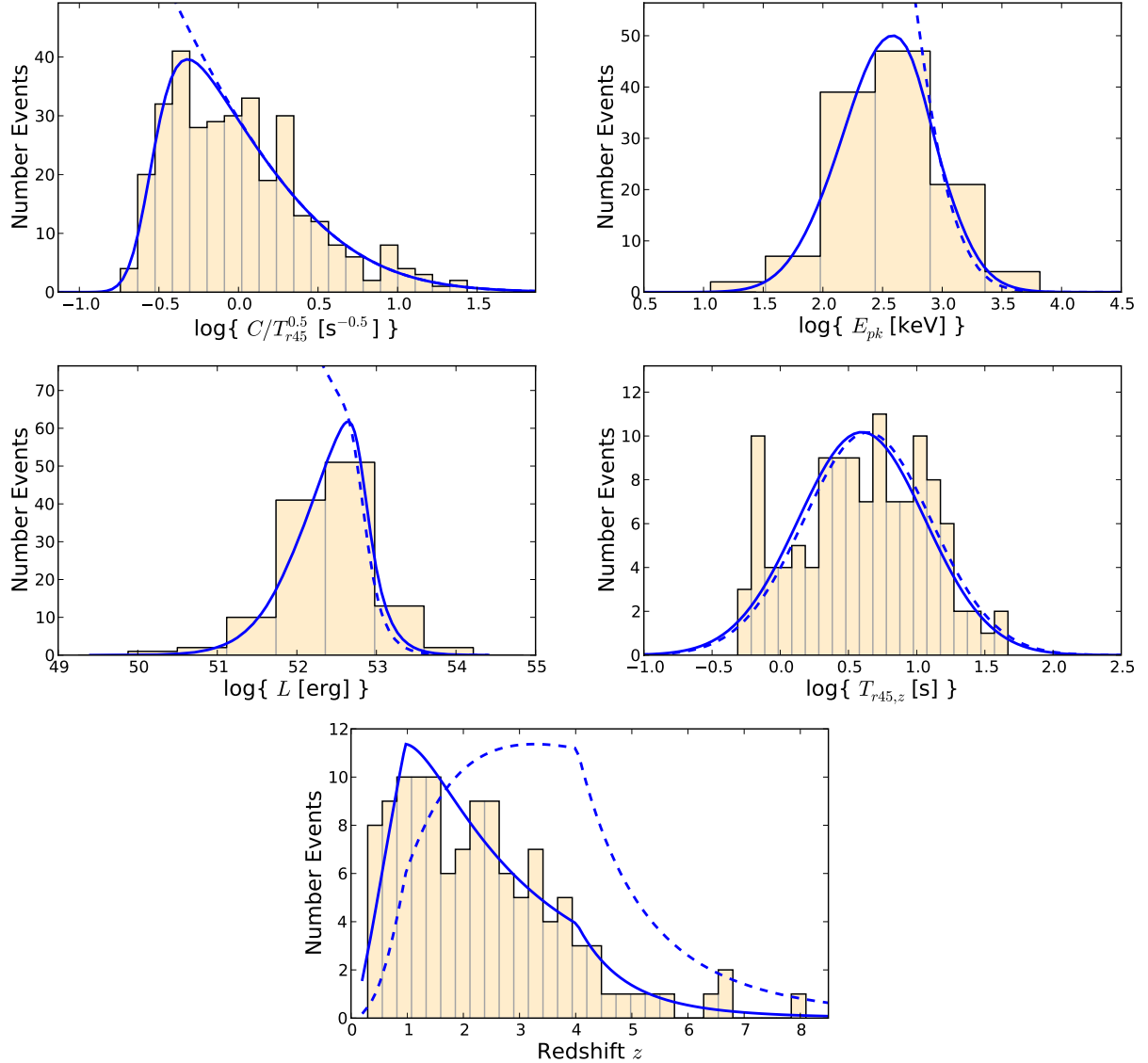


FIG. 2.— The best-fit GRB world model from Table 1 (left) superposed (solid lines) on the Swift data: counts C , redshift z , duration $T_{r45,z}$, hardness E_{pk} , and effective luminosity L (Section 2.2). The input models prior to convolution through the detector are plotted as dashed lines. The measured values for E_{pk} and L have large errors, with typical sizes that correspond to the bin widths used in the E_{pk} and L sub-panels. For all but the first sub-panel, the data and models are for GRBs with measured redshift only. Each curve provides an excellent fit to the data (Section 2.6). Note the large number of “missing” GRBs with low C , E_{pk} , and L .

al. (2005). The WXM sensitivity is comparable to that of Swift BAT; however, the total expected relative GRB rate is a factor ≈ 5 times lower due to an unfortunate mismatch in the HETE-2 instrument fields-of-view (see, e.g., Preger et al. 2001). Our resulting predicted $E_{pk,obs}$ curve for HETE-2 is an acceptable fit ($P_{KS} = 0.38$) to the observed data (see, Sakamoto et al. 2005). In Section 3.4 below, we further analyze the predicted $E_{pk,obs}$ distribution in the context of optimizing future GRB satellites to achieve maximal detection rates.

To check for pre-Swift consistency in the predicted E_{iso} distribution (Figure 5) we take the E_{iso} sample from Amati et al. (2006). Completing this sample by accounting for the heterogeneous satellite thresholds is a challenging task to perform rigorously. We assume, for simplicity, that the average threshold of pre-Swift satellites tracks

that of Swift but is a factor three times lower. This translates to a total relative rate factor (Swift to pre-Swift) of 2.5. We find that the shape of the predicted distribution agrees well with the observed shape (KS-test $P_{KS} = 0.37$).

In Paper I (also, Butler et al. 2009), we study in detail the correlation in Swift between E_{iso} and E_{pk} . Compared to pre-Swift studies (e.g., Amati et al. 2006), a log-log fit to the correlation appears to exhibit a (factor 2) increase in scatter and also a shift in normalization toward the Swift satellite threshold. This suggests (e.g., Nakar & Piran 2005; Band & Preece 2005) the possibility that the relation is actually an inequality: one region of the $E_{iso} - E_{pk}$ plane (lower left in Figure 6A) is physical and the other region is dominated by selection effects (upper right in Figure 6A). A number of recent stud-

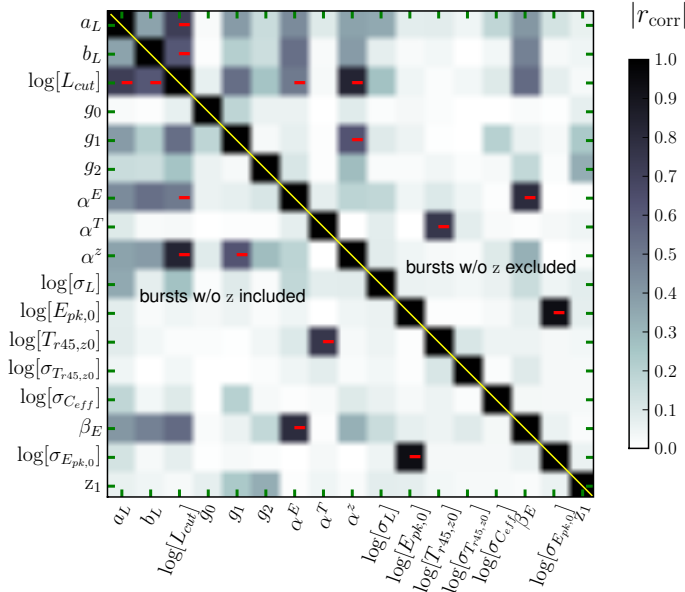


FIG. 3.— As demonstrated by the sample correlation matrix, the parameters are generally not strongly correlated (see, Section 2.6), thanks largely to the existence of measured redshifts. Here, we plot the matrix for all GRBs in the sample in the lower diagonal, and we plot the matrix for just GRBs with redshifts in the upper diagonal. Negative entries are marked with a red “-”.

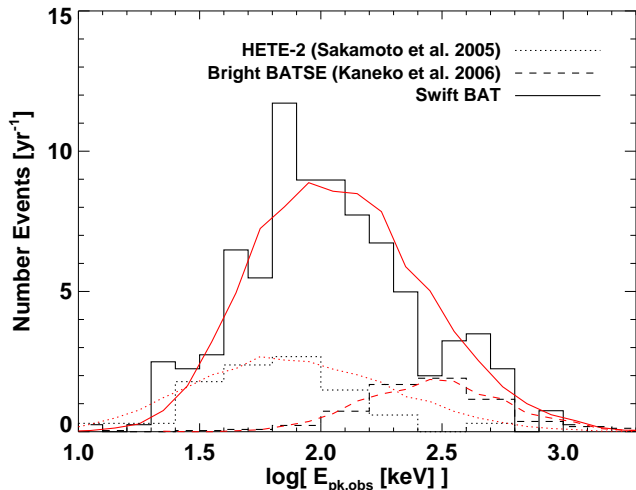


FIG. 4.— The predicted $E_{\text{pk,obs}}$ distributions for Swift (solid lines), BATSE (dashed lines), and HETE-2 (dotted lines) agree well with the observed data (Section 2.7).

ies have examined the instrument-dependent population of faint GRBs (Ghirlanda et al. 2008; Nava et al. 2008; Shahmoradi & Nemiroff 2009). The modelling here sheds new light on this controversial area of study.

As we summarize above, we have parameterized an intrinsic correlation via a log–log slope parameter α_E , which we find to be non-zero at a high level of statistical significance. The precise value of α_E depends sensitively on the rate of missing low- $E_{\text{pk,obs}}$ GRBs (Section 2.6).

It is important to stress that a $\alpha_E > 0$ does not trans-

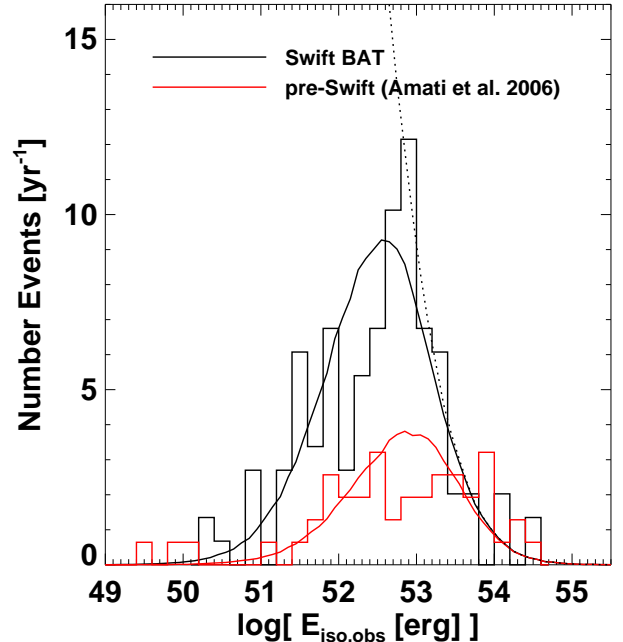


FIG. 5.— The predicted E_{iso} distributions for Swift (black) and pre-Swift data (red; taken from Amati et al. 2006) agree well with the observed data (Section 2.7). The dotted line shows the distribution without a detector cut-off: $\propto E_{\text{iso}}^{\alpha_L}$ below a smooth cutoff at $E_{\text{iso}} \lesssim 10^{53}$ erg.

late automatically into a strong observed correlation between E_{iso} and E_{pk} . That requires also a narrow distribution in the effective luminosity L , which governs the observed slope and scatter. Detected GRBs with $L \gtrsim L_{\text{cut}}$, will exhibit a strong correlation. However, if there are a significant number of GRBs extending to lower L as a powerlaw in L^{α_L} , these will asymptotically not show a correlation. Mathematically, this is because the luminosity function (Equation 2) becomes separable in E_{iso} and E_{pk} . A narrow log–log relation requires an effective luminosity function which is approximately a delta function. More quantitatively, we find we must have $\alpha_L > 2$ to generate a correlation with scatter $\lesssim 0.15$ dex in the Swift data. The Swift data rule out $\alpha_L > 2$ at the 6σ level ($-2\Delta \log(\mathcal{L}) = 40.2$ for one additional degree of freedom).

The expected behavior in the $E_{\text{iso}} - E_{\text{pk}}$ plane is summarized in Figure 6A, where we also compare to the Swift and pre-Swift data. At high E_{iso} , the relative rarity of high- E_{pk} events leads to a strong correlation relatively independent of the detector. However, at low- E_{pk} — due to the luminosity function tail — the correlation can exhibit a very large scatter. Pre-Swift GRBs appear to occupy the ridge of events in Figure 6A near $L = L_{\text{cut}}$. Swift has allowed us to sample well the broadening of L (see, also, Figure 2). The BATSE faint GRB sample (Nakar & Piran 2005; Band & Preece 2005) also appears to behave this way (Figure 6B).

The expected clustering of pre-Swift events near $L = L_{\text{cut}}$ can be demonstrated by applying the instrumental thresholds as above from Band (2003) to our model. As shown in Figure 6B, the breadth of L decreases as the

satellite sensitivity decreases. Also important is the relative lack of high- $E_{\text{pk,obs}}$ sensitivity for experiments like the WXM on HETE-2, which could permit the illusion that a true, narrow $E_{\text{iso}} - E_{\text{pk}}$ correlation extends to XRFs. The FWHM of the distribution in L is 0.4 dex for HETE-2 WXM as compared to 0.8 dex for Swift (and also for the faint BATSE sample).

The HETE-2 WXM distribution in L also has broad tails, which can make the observed distribution even narrower if tail events are falsely rejected as outliers. The same effect may also be seen for the E_{iso} distribution in Figure 5, where a few subluminal events in the pre-Swift sample (980425, 031203; e.g., Soderberg et al. 2004) appear to form the tail in the distribution including Swift events.

We note that we find evidence for a possible correlation with duration $T_{745,z}$ as in Firmani et al. (2006) for a considerably smaller sample (but, see, Collazzi & Schaefer 2008).

3. DISCUSSION & RESULTS

3.1. *Energetics vs. z*

We find a general tendency that high- z GRBs are intrinsically brighter and marginally softer in the observer frame than low- z GRBs (Figure 7). This arises predominantly due to the BAT flux limit, which corresponds to an increasing luminosity with z . Luminosity evolution (see below) does not play a strong role. We note that the redshift dependence of the observables is weak. If we ask, for example, what is the posterior prediction for the redshift of a burst of known z , we observe a large scatter between the predicted and true redshifts. However, weak decision rules can be obtained which may help identify high- z GRBs (see Figure 8).

Contrary to some previous studies (Section 1.1), we do not find significant evidence that the GRB luminosity function evolves with redshift. Although we have marginalized over the possibility of redshift evolution in E_{iso} , the extent of that evolution is weak $E_{\text{iso}} \propto (1+z)^{0.0 \pm 0.5}$ (Table 1).

We can test explicitly for strong luminosity evolution ($\alpha_z \geq 2$). We obtain fits which have a lower GRB rate density at intermediate and high redshift ($g_1 \approx -0.1$ instead of $g_1 > 1$ and $g_2 \approx -5$ instead of $g_2 \approx -3$ for $\alpha_z \approx 0$, with only modest change in the other model parameters; see also Section 2.6). However, the decreased quality of the fits ($-2\Delta\mathcal{L} = 25.1$ for 1 additional degree of freedom) — resulting from a relatively poorer fit to sample bright GRBs at low- z and faint GRBs at high- z — rules out $\alpha_z \geq 2$ at the 5σ level (see, Figure 9). To favor strong luminosity evolution, we would need to assume strong prior information that the GRB rate density follows more closely the cosmic star formation rate (see, Section 3.2).

3.2. *The GRB Comoving Rate Density*

The best-fit GRB rate density (Equation 5) — marginalized over GRB luminosity evolution, etc. — and uncertainty are shown in Figure 10. We find that the $z \lesssim 1$ slope g_0 appears to track that of star formation well. This fact can be used to approximately normalize the relation at $z = 1$. A rigorous normalization is not possible here, because the Swift data do not constrain

the number of GRBs at the faint end of the luminosity function nor is the beaming fraction $\langle f_{\text{beam}} \rangle$ well-constrained. We can also quote a normalization above a given intrinsic flux level: the all-sky intrinsic rate of long-duration GRBs with $E_{\text{iso}} > 10^{52}$ erg is $10^{3.1 \pm 0.3}$ GRBs $\langle f_{\text{beam}} \rangle^{-1} \text{ yr}^{-1}$ (or $10^{-2.4 \pm 0.5}$ GRBs $\langle f_{\text{beam}} \rangle^{-1} \text{ yr}^{-1} \text{ Gpc}^{-3}$ at $z = 0$). Integrating the SFR over volume and considering a Salpeter IMF (e.g., Dahlen & Fransson 1999) with GRB progenitors more massive than $20 M_{\odot}$ (e.g., Fryer 1999), only about 0.1% [$\langle f_{\text{beam}} \rangle / 0.01$] of massive stars explode as bright GRBs (see, also, e.g., Soderberg et al. 2005). Numbers increase mildly to low E_{iso} levels $\propto E_{\text{iso}}^{-0.36 \pm 0.07}$.

Beyond $z = 1$, the GRB rate increases significantly faster than star formation. At $z = 6$ the GRB rate is roughly two orders of magnitude greater, although the star formation rate is quite uncertain at such high redshift. The GRB rate enhancement relative to star formation, which we derive for $z = 1 - 4$, is closely consistent with that found by Kistler et al. (2008) using a smaller Swift sample and not fitting for the possibility of GRB luminosity evolution.

Kistler et al. (2008) discuss a number of possible scenarios which could yield that evolution (decreasing cosmic metallicity with z , an initial mass function for stars which becomes increasingly skewed toward more massive stars at high- z , etc.), but conclude that no scenario adequately describes the data without fine-tuning. Salvaterra & Chincarini (2007) (also, Modjaz et al. 2008; Salvaterra et al. 2009a,b) have explored one such fine-tuning scenario — a preference for GRBs to arise in metal-poor host galaxies (e.g., Savaglio 2006; Stanek et al. 2006), resulting in a metallicity cutoff $Z < Z_{\text{th}} \approx 0.1 Z_{\odot}$. Following Salvaterra & Chincarini (2007) (also, Langer & Norman 2006), we can use the prescription from Kewley & Kobulnicky (2005) for how metallicity evolves with redshift to estimate the mass density Σ evolution:

$$\Sigma(z) = \frac{\hat{\Gamma}[0.84, (Z_{\text{th}}/Z_{\odot})^2 10^{0.3z}]}{\Gamma(0.84)}, \quad (8)$$

where $\hat{\Gamma}$ (Γ) is the incomplete (complete) gamma function, $\dot{\rho}(z) \propto \Sigma(z)\dot{\rho}(z)_{\text{SFR}}$. This translates into a $\dot{\rho}(z)$ that peaks at higher z than $\dot{\rho}_{\text{SFR}}$.

Salvaterra & Chincarini (2007) (also, Salvaterra et al. 2009a) decide that luminosity evolution (a possibility we rule out at the 5σ level; Section 3.1) fits the data better than a strong metallicity cutoff $Z_{\text{th}}/Z_{\odot} = 0.1$. However, we find that a more relaxed cutoff (Z_{th}/Z_{\odot} in the range 0.2–0.5; Figure 10) appears to describe the data quite well. A higher cutoff is also more consistent with studies of the GRB host galaxy mass distribution (e.g., Kocevski et al. 2009). The apparently smooth continuation of the rate density above $z = 4$ suggests the presence of no new evolutionary effects (see, also, Kistler et al. 2009). The uncertainty is large, however. It is possible that Pop. III stars may begin to contribute at this epoch, although, our observed rates (Section 3.4 below) are marginally inconsistent with the prediction from Bromm & Loeb (2002) of 10% of Swift GRBs at $z > 5$.

3.3. *The z Distribution for GRBs Without z*

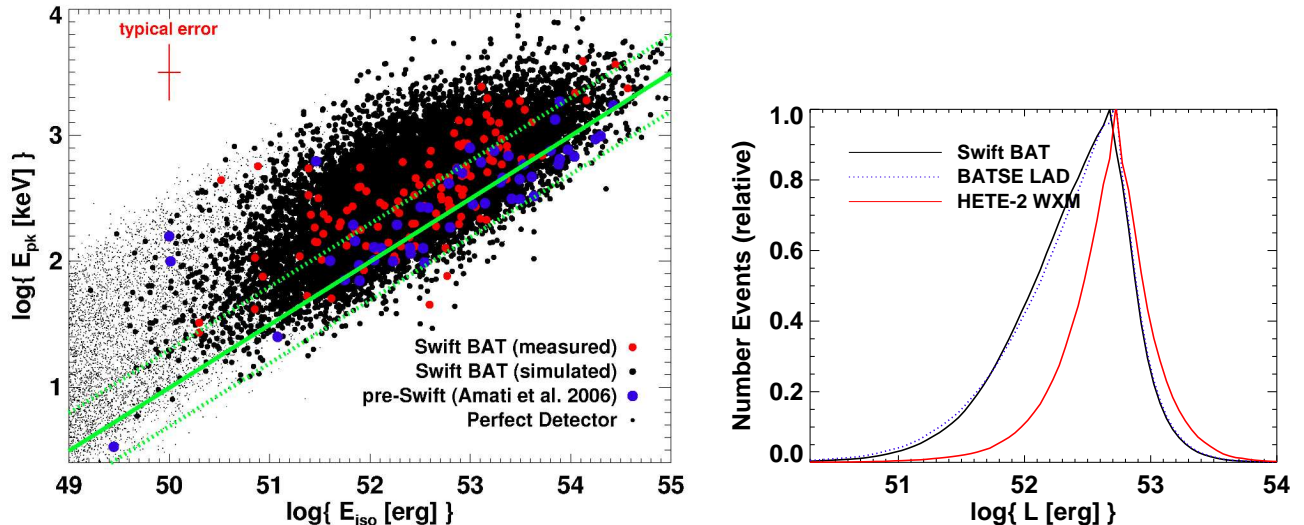


FIG. 6.— The predicted $E_{\text{iso}} - E_{\text{pk}}$ distributions (A) and normalization (B) for multiple missions. Due to the presence of faint GRBs which sample the low energy tail of the luminosity function (Section 2.7, Swift and BATSE are expected to yield (A) a broad $E_{\text{iso}} - E_{\text{pk}}$ correlation (as observed, e.g., Nakar & Piran 2005; Band & Preece 2005; Butler et al. 2007), which increases in breadth as E_{pk} decreases. Bright GRBs, from the least sensitive satellites, are expected to yield a tight correlation (as observed, e.g., Amati et al. 2002, 2006). The best-fit pre-Swift correlation and scatter are marked with green lines. The normalization of the correlation (B) — plotted most naturally here including duration and redshift (which contribute weakly to the observed shape) — is shown to exhibit a strong decrease (factor 2) in scatter in HETE-2 as opposed to Swift or BATSE. A typical error bar for Swift is plotted in red in the upper left of sub-panel A.

We have ignored in the above analysis the potential selection effects associated with obtaining spectroscopic host redshifts (e.g., Bloom 2003). In principle, relative to pre-Swift experiments, arcsecond X-ray positions from the XRT for nearly all GRBs (e.g., Butler 2007) should translate into a higher optical followup and detection rate. However, it remains true in the Swift era that 25–50% of all GRBs exhibit suppressed optical flux relative to X-ray flux or are undetected (“dark” GRBs; e.g., Jakobsson et al. 2004; Melandri et al. 2008; Cenko et al. 2009a; Zheng et al. 2009) despite deep followup. We have redshifts for only 37% of Swift GRBs. The distribution of these redshifts depends, in principle, not just on the intrinsic distribution but also on the complicated details of GRB afterglow observability (location in the sky, time of month, etc.; see, e.g., Jakobsson et al. 2005) and also on the relative interest of particular observers to expend valuable resources on GRBs lying at a given potential redshift. We explore here the biases these effects could introduce.

We have conducted a number of 2-sample KS tests to check consistency between the distributions of parameters in Tables 3 & 4 for GRBs with $T_{90} > 3$ s. The duration statistics show no signs of strong disagreement ($P > 0.7$). There is modest evidence ($P = 0.1$) for difference in the 15–350 keV fluences (also present for the bolometric fluence and $E_{\text{pk,obs}}$). We do note that the events without z are on average about 50% fainter. These events could be fainter because they, on average, have lower intrinsic luminosity or because they are at higher z (or a combination of the two). That such a large fraction of events shows this flux variation suggests a range of source redshifts and the probability that most correspond to $z \approx 1 - 3$ where the observable Universe has most of its volume.

We can investigate a spectroscopic redshift selection bias by fitting for it explicitly. Here, we imagine that $\dot{\rho}(z)_{\text{no-}z} = \dot{\rho}(z)$, the true rate density, while $\dot{\rho}(z)_z = \epsilon(z)\dot{\rho}(z)$, where $\epsilon(z)$ is a function describing the optical detection and spectroscopy rate of GRBs and their host galaxies versus z . We allow $\dot{\rho}(z)_{\text{no-}z}$ and $\dot{\rho}(z)_z$ to have different slopes g_1 and g_2 describing the intermediate and high- z populations. It is reasonable to expect spectroscopy to achieve high recovery rates ($\epsilon(z)$ not decreasing) below $z = 1$ (e.g., Bloom 2003).

We find that these extra two degrees of freedom in the modelling allow for a meager 1σ improvement in the fit ($-2\Delta\mathcal{L} = 2.74$). Similar to the argument above based on concordance of fit parameters, this tells us that the sample without z does not strongly demand a different $\dot{\rho}(z)$. However, to what extent *could* the distributions differ and how does this impact our conclusions? The best-fit slopes for $\dot{\rho}(z)_{\text{no-}z}$ ($g_1 = 0.75, g_2 = -3.6$) are modestly lower than those for $\dot{\rho}(z)_z$ ($g_1 = 1.2, g_2 = -2.7$), indicating a bias $\epsilon(z) \sim (1+z)^{0.5}$ against obtaining redshifts for low-, rather than high- z GRBs. Marginalizing over the extra parameters, we find that $\dot{\rho}(z)$ is affected at the $< 10\%$ level for $z = 1 - 4$. Therefore, our constraints above on density evolution are practically unaffected.

The bias has a modest effect on the predicted rates of high redshift GRBs below: $(30 \pm 30)\%$ fewer $z > 6$ GRBs are expected in the full Swift (or EXIST) sample as compared to assuming that $\epsilon(z)$ is independent of z . The extra uncertainty in the rates resulting from marginalizing over ϵ is small compared the uncertainty already present at high- z . The reader should be warned, however, that — due to the small sample size at high- z — we cannot be sure that our parameterization of ϵ is sufficiently robust to reliably account for high- z rate variations.

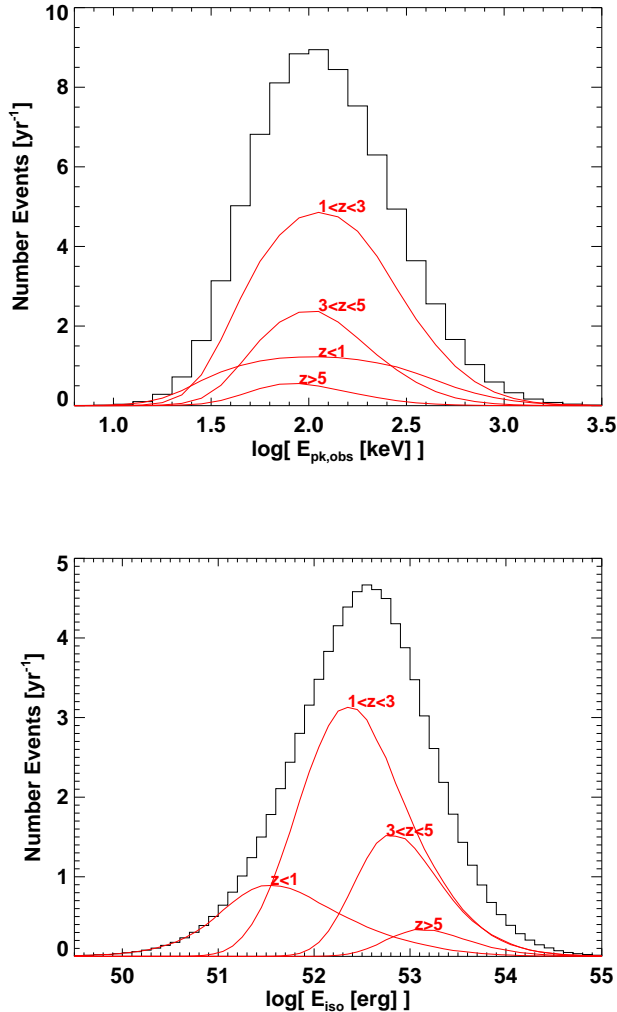


FIG. 7.— The predicted variation of E_{iso} and $E_{\text{pk,obs}}$ observed by Swift with redshift z is weak. High redshift (e.g., $z > 5$) GRBs are systematically, intrinsically brighter than low- z GRBs. This is due primarily to the BAT flux limit, which corresponds to an increasing E_{iso} with increasing z , and not luminosity evolution, which is not significantly present in the Swift sample.

The most natural explanation for — or at least a strong contributor to — the apparent lack of low spectroscopic redshifts may be the so called “redshift desert” at $1.5 \lesssim z \lesssim 2$ (the observed rate does in fact show a decrement here; Figure 2; see also, Coward et al. 2008). There is a lack of strong star-formation emission lines in the optical bands for galaxies observed in this redshift range. It is possible to obtain redshift in this range (detected, e.g., through Mg II absorption of bright afterglow light), but host galaxy redshifts will be very challenging to obtain for faint afterglows or those observed too late. It is quite likely that some or many Swift GRBs without spectroscopic redshifts have true redshifts preferentially in the range $1.5 < z < 2$. Deep host galaxy imaging studies (e.g., Perley et al. 2009a; Fynbo et al. 2009) can shed important light on this possibility, because these hosts may in general be detectable with modest imaging investments.

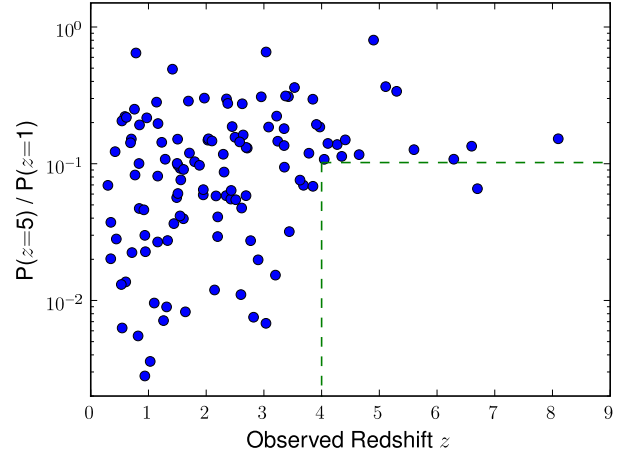


FIG. 8.— Ratio of the posterior probability at $z = 5$ to that at $z = 1$ for Swift bursts of known redshift z . There is a large scatter and only a weak correlation. Weak decision rules can be obtained, however, resulting from the relative observer-frame faintness of high- z GRBs above Swift threshold: nearly all (13/14) bursts at $z > 4$ fall above the median $P(z=5)/P(z=1)$ value for $z < 4$ (dashed lines). This allows a potential factor two target reduction for high- z followup.

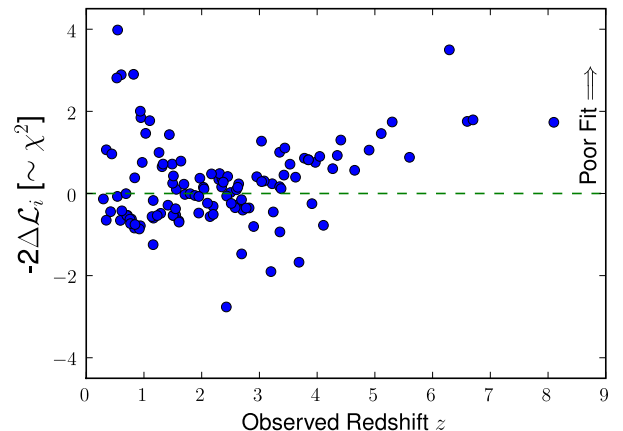


FIG. 9.— Decrease in the relative quality of fit $-2\Delta \log(\mathcal{L}_i)$ (Equation A-5) for the best-fit model with strong luminosity evolution ($\alpha_z \equiv 2$) relative to the best-fit overall model ($\alpha_z \approx 0$; no evolution). The y -axis scales approximately as $\Delta \chi^2 \approx \sigma^2$ and is plotted for each GRB as a function of z . The fit quality, considering strong luminosity evolution, is systematically poor at low- and high- z , although there are a few GRBs at intermediate z which appear to prefer evolution. The overall evidence in disfavor of strong luminosity evolution is $-2 \sum \Delta \log(\mathcal{L}_i) = 25.1$ (5σ ; Section 3.1).

3.4. Towards a Better Mousetrap: EXIST

In this section, we utilize the best-fit Swift GRB model (Table 1, left) to estimate the number of GRBs Swift — and a more sensitive future Swift-like experiment — will detect as a function of z . EXIST (e.g., Grindlay et al. 2009), to a reasonable approximation, with BAT-like CZT detectors and trigger software, is a scaled-up (i.e., more sensitive) Swift BAT (see, e.g., Band 2003; Band et al. 2008). We take the sensitivity increase to be a factor 7.2 and the field of view to be the same at the BAT (Josh

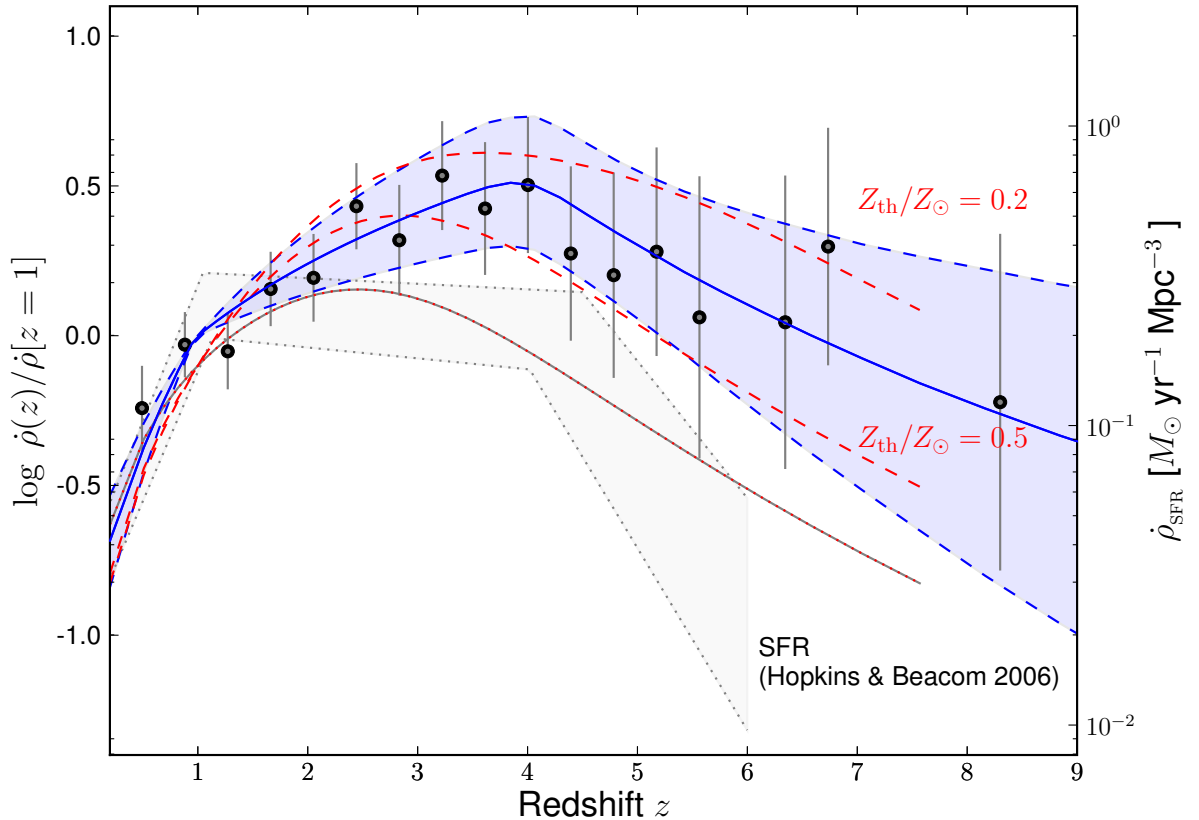


FIG. 10.— The comoving rate density, relative to the rate density at $z = 1$. Dashed lines give the 90% confidence regions for the best fit (blue) curve. Also plotted is the location of star formation rate (SFR) data (gray hatched region) and a parameterized fit (solid gray curve) from (Hopkins & Beacom 2006). We use this fact that the GRB rate traces well the SFR at $z < 1$ to normalize the GRB rate (right y -axis). Following (Salvaterra & Chincarini 2007), the red dashed curves show plausible enhancements to the gray SFR curve resulting from a metallicity cutoff: GRB hosts have $Z < Z_{\text{th}}$.

TABLE 2
PREDICTED REDSHIFT RATES [YR⁻¹]

	Swift	EXIST
all- z	89 ± 8	270 ± 40
$5 < z < 8$	4.4 ± 2.4	$17.4 (-7.6, +8.5)$
$8 < z < 12$	$0.5 (-0.5, +0.9)$	$2.3 (-2.1, +3.7)$
$z > 5$	$5.0 (-2.8, +3.3)$	$20.2 (-9.6, +13.5)$
$z > 6$	$2.3 (-1.8, +2.3)$	$9.6 (-6.2, +10.1)$
$z > 7$	$1.1 (-1.1, +1.6)$	$5.0 (-3.9, +7.3)$
$z > 8$	$0.6 (-0.6, +1.1)$	$2.8 (-2.5, +5.3)$
$z > 10$	$0.2 (-0.2, +0.6)$	$1.0 (-1.0, +2.9)$
$z > 12$	$0.1 (-0.1, +0.4)$	$0.5 (-0.5, +1.7)$

Note.—Rates (90% Conf.) for long duration $T_{90} > 3$ s GRBs only. Short-duration GRB rates are discussed in Section 3.4.

Grindlay, private communication).

Figure 11 shows the expected rate of detectable long-duration ($T_{90} > 3$ s) GRBs for Swift — if redshifts were measured for all Swift GRBs — and for EXIST (see, also, Table 2). About 3–9% (4–13%) of all Swift (EXIST) GRBs are expected to lie at high redshift ($z > 5$). Our prediction is consistent with, but on the low side of, that found by Jakobsson et al. (2005, 2006) (5–40%

of Swift GRBs at $z > 5$) from a survival analysis of a sub-sample of Swift GRBs with uniform optical followup properties and redshifts (or redshift constraints). Our numbers agree well with those presented in Salvaterra et al. (2008), provided we correct the EXIST field-of-view from Salvaterra et al. (2008) to be 1.4 sr instead of 5 sr. Our numbers also agree well with independent estimates based on host-galaxy observations of optically dark GRBs (0.2–14% {0.2–7%} of Swift GRBs at $z > 5$ { $z > 7$ } Perley et al. 2009a, see Figure 11).

The relative EXIST/Swift rate increases with increasing redshift (subpanel Figure 11). This can be understood as the result of the $E_{\text{iso}} - E_{\text{pk}}$ correlation and the redshift dependence of the flux (Figure 7) — a more sensitive satellite detects fainter, softer GRBs, and these tend to be preferentially at higher redshift. The strong difference in expected rate-increase-versus-hardness is most clearly seen in a plot of the Swift logN–logS (e.g., Figure 1). We observe that faint, hard GRBs are becoming increasingly rare, while faint, soft GRBs are growing strongly in number. It is also interesting to note (see, Figure 1) that the short GRB rate appears to be steeply rising to low flux levels. This suggests that EXIST may see a factor ten more short GRBs ($\gtrsim 120 \text{ yr}^{-1}$) than Swift, extending the observed short-duration GRB red-

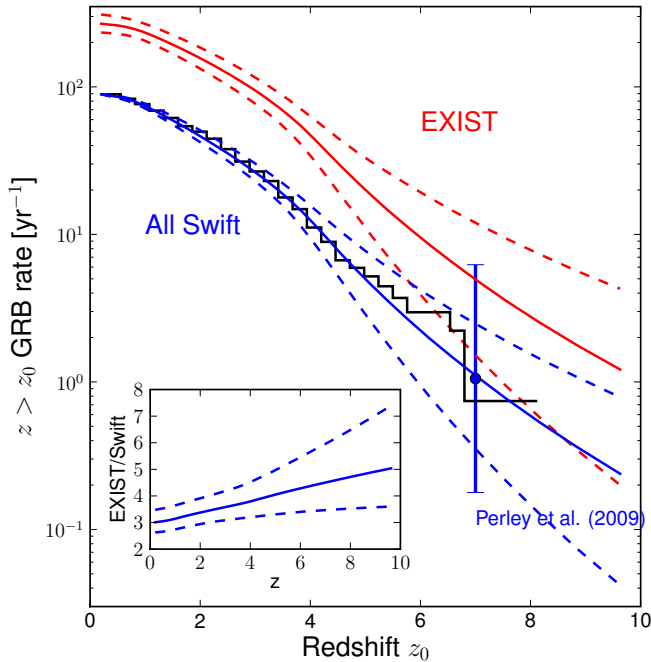


FIG. 11.— The observed (black) and predicted redshift rates for Swift (blue) and EXIST (red) GRBs. The 90% confidence intervals are marked with dashed lines (see, also, Table 2). The plot subpanel demonstrates the increasing, relative sensitivity of EXIST at high z by showing the relative number of predicted GRBs above redshift z . The blue point from Perley et al. (2009a) is an independent measurement based on optical studies of optically-dark GRB host galaxies.

shift sample to intermediate and possibly high- z .

We now explore the characteristics of an optimal GRB detector, so constructed as to maximize the number of detected GRBs. First, it is important to note that a large sensitivity increase (factor 7.2 for EXIST relative to Swift) results in only a factor $\approx 3 - 4$ increase in rates due to the shallowing out of the $\log N - \log S$ (Figure 1). Therefore, field-of-view increase should be prioritized over sensitivity increase. Second, it is clearly important to be able to trigger over a broad range of timescales (e.g., Band 2006). Finally, the analysis above allows us to make general recommendations regarding spectral sensitivity. The observed peak in $E_{\text{pk,obs,max}}$ in the $E_{\text{pk,obs}}$ distribution is at ≈ 100 keV for Swift. If we imagine a hypothetical detector which is S_{rel} times more sensitive than Swift, then we observe that the peak in the $E_{\text{pk,obs}}$ distribution decreases as $E_{\text{pk,obs,max}} \propto S_{\text{rel}}^{-1/4}$. Consistently, as the peak decreases, 90% of all GRBs have $E_{\text{pk,obs}} < E_{\text{pk,max}}/3$. The rate of GRBs with $E_{\text{pk,obs}} = 10$ keV relative to those with $E_{\text{pk,obs}} = 100$ keV, for example, increases strongly as $\approx S_{\text{rel}}^2$. That is, a doubling of S_{rel} results in about three times more $E_{\text{pk,obs}} = 10$ keV bursts and only about 30% more $E_{\text{pk,obs}} = 100$ keV GRBs (see also, Figure 1). It does not help to increase sensitivity to hard GRBs, because these are rare. Optimizing for high GRB rates means optimizing for soft GRBs. A satellite which detects soft GRBs well is also an efficient high- z machine, because

high- z GRBs have lower than average $E_{\text{pk,obs}}$ (Figure 7).

4. CONCLUSIONS

We have exploited a careful modelling of the Swift BAT trigger threshold — strongly dependent on burst hardness and duration — to derive constraints on the GRB intrinsic distributions in E_{iso} , E_{pk} , $T_{r45,z}$, and z . This is the first study, utilizing a uniform reduction of the largest available number of Swift GRBs, to rigorously propagate GRB measurement errors and their covariances (through very general functional forms describing the intrinsic distributions) to obtain reliable confidence intervals for the rates. The modelling is now possible thanks to the large number of spectroscopic redshifts for Swift GRBs which largely alleviate parameter degeneracies.

We find that the GRB luminosity function is best written as a broken powerlaw (Table 1) in the effective luminosity

$$L = \frac{E_{\text{iso}}}{(1+z)^{0.0 \pm 0.5}} \left(\frac{10^{2.5} \text{keV}}{E_{\text{pk}}} \right)^{1.8 \pm 0.3} \left(\frac{10^{0.6} \text{s}}{T_{r45,z}} \right)^{0.4 \pm 0.2}. \quad (9)$$

The distribution $\tilde{\phi}(L) = dN/d\log L$ is nearly flat $\propto L^{-0.2 \pm 0.2}$ below $\log(L_{\text{cut}}) = 52.7 \pm 0.4$ and declines sharply thereafter $\propto L^{-3.0 \pm 1.5}$. Our multivariate GRB world model, which includes this luminosity function to produce very different intrinsic rates for hard or soft-spectrum GRBs (as observed, e.g., Figure 1), accurately reproduces both Swift and pre-Swift rates, and should be very useful for future simulation studies. We note that the overall rate versus redshift does not appear to strongly depend on the multivariate modelling.

We draw the following principle conclusions:

- There is a real, intrinsic correlation between E_{iso} and E_{pk} (and possibly also $T_{r45,z}$), despite indications in our previous work (Paper I) that this might be solely due to a selection effect. However, the correlation *is not* a narrow log-log relation (e.g., Amati et al. 2008), and its observed appearance (more like an inequality) is strongly detector-dependent.
- We find modest ($\sim 3\sigma$) evidence for a large population of low- $E_{\text{pk,obs}}$ GRBs (XRFs; see, also Strohmayer et al. 1998; Lamb et al. 2005), and future satellites may overwhelmingly detect these, as well as a potentially large missing (from Swift) population of short-duration GRBs.
- The Swift sample does not require luminosity evolution to produce the observed number of GRBs at high- z . In fact, we rule out the possibility of strong evolution at the 5σ level.
- An increase in the GRB rate relative to the SFR at $z > 1$ appears to be due evolution in the rate density, and the shape of this evolution is roughly consistent with that expected from a preference for GRBs to reside in modestly low-metallicity ($Z \lesssim 0.3Z_{\odot}$) environments.
- Finally, the predicted observed rate of GRBs at high- z (3 – 9% at $z > 5$) is consistent with, if marginally lower than that found in previous studies.

The conclusions above are based primarily on the high-energy properties of Swift GRBs, without detailed consideration of the afterglow properties or optical selection biases (but see Section 3.3). This is good in the sense that our rate estimates will be largely independent of those based primarily on afterglow or host galaxy studies (e.g., Perley et al. 2009a; Fynbo et al. 2009). However, we are fundamentally limited in firmly extending our conclusions to include all GRBs by the fact that a majority of Swift GRBs lack measured redshifts. We note that redshift limits are easily incorporated into the formalism we have developed; however, our initial calculations suggest there are currently too few (about 20% for dark GRBs Jakobsson et al. 2005, 2006) to significantly improve or modify our results. Also, useful would be constraints on the highest energy emission from simultaneous observations from other satellites (e.g., Bellm et al. 2008; Krimm et al. 2009). These would help limit the sharpness of the luminosity function cutoff L_{cut} to help

infer the breadth of the intrinsic luminosity distribution and also better limit the potential of luminosity evolution. Finally, it will be important to better constrain the role of GRB beaming and the way this shapes the distributions in numbers, E_{iso} , E_{pk} , etc. (e.g., Guetta et al. 2005; Lamb et al. 2005). Given apparent challenges in inferring beaming from imaging observations of X-ray and optical afterglows (e.g., Racusin et al. 2009, and references therein), it may be most fruitful to focus on late-time radio observations (e.g., Cenko et al. 2009c).

We thank D. Perley, D. Kocevski, B. Cenko, M. Kistler, and N. Gehrels for comments on the manuscript and for useful discussions. Greatly appreciated also were helpful comments and criticisms from an anonymous referee. NRB is supported through the GLAST Fellowship Program (NASA Cooperative Agreement: NNG06DO90A). D.P. is partially supported by US Department of Energy SciDAC grant DE-FC02-06ER41453.

REFERENCES

- Amati, L., et al. 2002, *A&A*, 390, 81
 Amati, L. 2006, *MNRAS*, 372, 233
 Amati, L. 2008, *MNRAS*, 391, 577
 Band, D. 1992, *ApJ*, 400, L63
 Band, D. L. 2003, *ApJ*, 588, 945
 Band, D. L. 2006, *ApJ*, 644, 378
 Band, D. L., et al. 1993, *ApJ*, 413, 281
 Band, D. L., et al. 2008, *ApJ*, 588, 945
 Band, D. L., & Preece, R. D. 2005, *ApJ*, 627, 319
 Barthelmy, S. D., et al. 2005, *Space Science Reviews*, 120, 143
 Bellm, E. C., et al. 2008, arXiv:0801.2417
 Berger, E., et al. 2008a, GCN #8335
 Berger, E., et al. 2008b, GCN #8434
 Berger, E., & Rauch, M. 2008, GCN #8542
 Bloom, J. S. 2003, *AJ*, 125, 2865
 Bromm, V., & Loeb, A. 2002, *ApJ*, 575, 111
 Burrows, D. N., et al. 2005, *Space Science Reviews*, 120, 165
 Butler, N. R. 2007, *AJ*, 133, 1027
 Butler, N. R., et al. 2007, *ApJ*, 671, 565 (Paper I)
 Butler, N. R., et al. 2009, *ApJ*, 694, 76
 Cenko, S. B., et al. 2007a, GCN #6556
 Cenko, S. B., et al. 2007b, GCN #6888
 Cenko, S. B., et al. 2009a, *ApJ*, 693, 1484
 Cenko, S. B., et al. 2009b, GCN #9518
 Cenko, S. B., et al. 2009c, *ApJSubmitted*, arXiv:0905.0690
 Chornock, R., et al. 2009a, GCN #8994
 Chornock, R., et al. 2009b, GCN #9151
 Chornock, R., et al. 2009c, GCN #9243
 Choudhury, T. R., & Srianand, R. 2002, *MNRAS*, 336, L27
 Cohen, E., & Piran, T. 1995, *ApJ*, 444, L25
 Collazzi, A. C., & Schaefer, B. E. 2008, *ApJ*, 688, 456
 Coward, D. M., et al. 2008, *MNRAS*, 386, 111
 Cucchiara, A., et al. 2007a, GCN #6665
 Cucchiara, A., et al. 2007b, GCN #7124
 Cucchiara, A., & Fox, D. B. 2008, GCN #7654
 Cucchiara, A., et al. 2008a, GCN #8065
 Cucchiara, A., et al. 2008b, GCN #8713
 Daigne, F., et al. 2006, *MNRAS*, 372, 1034
 D'Avanzo, P., et al. 2007, GCN #7152
 D'Avanzo, P., et al. 2008a, GCN #7997
 D'Avanzo, P., et al. 2008b, GCN #8350
 Dahlen, T., & Fransson, C. 1999, *A&A*, 350, 349
 D'Elia, V., et al. 2008a, GCN #8438
 D'Elia, V., et al. 2008b, GCN #8531
 de Ugarto Postigo, A., et al. 2009a, GCN #9383
 de Ugarto Postigo, A., et al. 2009b, GCN #9771
 de Ugarto Postigo, A., et al. 2009c, GCN #8766
 Efron, B. & Petrosian, V. 1992, *ApJ*, 399, 345
 Fatkhullin, T., et al. 2009, GCN #9712
 Fenimore, E. E., & Bloom, J. S. 1995, *ApJ*, 453, 25
 Fenimore, E. E., et al. 1995, *ApJ*, 448, L101
 Fenimore, E. E., & Ramirez-Ruiz, E. 2000, *ApJSubmitted*, astro-ph/0004176
 Firmani, C., et al. 2004, *ApJ*, 611, 1033
 Firmani, C., et al. 2006, *MNRAS*, 370, 185
 E., Fox, D. B., & Cucchiara, A. 2007, GCN #6470
 Fryer, C. L. 1999, *ApJ*, 522, 413
 Fugazza, D., et al. 2009, GCN #8892
 Fynbo, J. P. U., et al. 2008a, GCN #7797
 Fynbo, J. P. U., et al. 2008b, GCN #7949
 Fynbo, J. P. U., et al. 2008c, GCN #8225
 Fynbo, J. P. U., et al. 2008d, GCN #8254
 Fynbo, J. P. U., et al. 2009, *ApJS Accepted*, arXiv:0907.3449
 Gehrels, N., et al. 2004, *ApJ*, 611, 1005
 Gelman, A., et al. 2004, *Bayesian Data Analysis* (2nd ed.; Boca Raton: Chapman & Hall/CRC)
 Ghirlanda, G., Ghisellini, G., & Lazzati D. 2004, *ApJ*, 616, 331
 Ghirlanda, G., et al. 2008, *MNRAS*, 387, 319
 Gorosabel, J., et al. 2004, *A&A*, 427, 87
 Graham, J. F., et al. 2007, GCN #6836
 Gregory, P. 2005, *Bayesian Logical Data Analysis for the Physical Sciences*, Cambridge University Press, Cambridge
 Greiner, J., et al. 2008, arXiv:0811.4291
 Grindlay, J., et al. 2009, in *Proc. Huntsville Gamma-ray Burst Symposium*, AIPC (C. Meegan, N. Gehrels and C. Kouveliotou, eds.), 18
 Guetta, D., et al. 2005, *ApJ*, 619, 412
 Hartmann, D. H., & The, L.-S. 1993, *A&AS*, 97, 219
 Heise, J., et al. 2001, in *Proc. Second Rome Workshop: Gamma-ray Bursts in the Afterglow Era*, ed. E. Costa, F. Frontera, & J. Hjorth (Berlin: Springer), 16
 Higdon, J. C. & Schmidt, M. 1990, *ApJ*, 355, 13
 Hjorth, J., et al. 2003, *Nature*, 423, 847
 Hopkins, A. M., & Beacom, J. F. 2006, *ApJ*, 651, 142
 Horack, J. M., & Hakkila, J. 1997, *ApJ*, 479, 371
 Houck, J. C., & Denicola, L. A. 2000, in *ASP Conf. Proc.*, 216, 591
 Hurley, K. in *AIP Conf. Proc.*, Vol. 265, *Gamma-ray Bursts*, ed. W. C. Paciesas & G. J. Fishman (New York: AIP), 3
 Jakobsson, P. et al. 2004, *ApJ*, 617, L21
 Jakobsson, P. et al. 2005, *A&A*, 447, 897
 Jakobsson, P. et al. 2006, in *AIP Conf. Proc* 836, *Gamma-ray Bursts in the Swift Era*, ed. S. S. Holt, N. Gehrels, J. A. Nousek, 552
 Jakobsson, P., et al. 2007a, GCN #6952
 Jakobsson, P., et al. 2007b, GCN #7117
 Jakobsson, P., et al. 2008a, GCN #7286
 Jakobsson, P., et al. 2008b, GCN #7757
 Jakobsson, P., et al. 2008c, GCN #7832
 Jakobsson, P., et al. 2008d, GCN #8077
 Kaneko, Y., et al. 2006, *ApJS*, 166, 298

- Kewley, L., & Kobulnicky, H. A. 2005, in *Starburst: From 30 Doradus to Lyman Break Galaxies*, ed. R. de Grijs & R. M. González Delgado (Dordrecht: Springer), 307
- Kistler, M. D., et al. 2008, *ApJ*, 673, L119
- Kistler, M. D., et al. 2009, Accepted to *ApJ*, arXiv:0906.0590
- Kocevski, D., & Liang, E. 2006, *ApJ*, 642, 371
- Kocevski, D., & Butler, N. R. 2008, *ApJ*, 680, 531
- Kocevski, D., et al. 2009, *ApJ*, 702, 377
- Kouveliotou, C., et al. 1993, *ApJ*, 413, L101
- Krimm, H. A., et al. 2009, *ApJ*, 704, 1405
- Lamb, D. Q., et al. 2004, *New A Rev.*, 48, 459
- Lamb, D. Q., et al. 2005, *ApJ*, 620, 355
- Lamb, D. Q., & Reichart, D. E. 2000, *ApJ*, 536, 1
- Landsman, W., et al. 2008, GCN #8601
- Langer, N. & Norman, C. A. 2006, *ApJ*, 638, L63
- Ledoux, C., et al. 2007, GCN #7023
- Levesque, E. M., et al. 2009, *MNRAS Accepted*, arXiv:0907.1661L
- Levesque, E., et al. 2009, GCN #9264
- Lloyd, N. M., Petrosian, V., & Malozzi, R. S. 2000, *ApJ*534, 227
- Lloyd-Ronning, N. M., et al. 2002, *ApJ*, 574, 554
- Loredo, T. J., & Wasserman, L. M. 1995, *ApJS*, 96, 261
- Loredo, T. J., & Wasserman, L. M. 1998, *ApJ*, 502, 75
- Lynden-Bell, D. 1971, *MNRAS*, 155, 95
- Madau, P., et al. 1996, *MNRAS*, 283, 1388
- Malesani, D., et al. 2007, GCN #6651
- Malesani, D., et al. 2008, GCN #7544
- Malesani, D., et al. 2009a, GCN #9457
- Malesani, D., et al. 2009b, GCN #9761
- Maloney, A., & Petrosian, V. 1999, 518, 32
- Meegan, C. A., et al. 1992, *Nature*, 355, 143
- Melandri, A., et al. 2008, *ApJ*, 686, 1209
- Metzger, M. R., et al. 1997, *Nature*, 387, 878
- Modjaz, M., et al. 2008, *ApJ*, 135, 1136
- Murakami, T., et al. 2003, *PASJ*, 55, L65
- Nakar, E., & Piran, T. 2005, *MNRAS*, 360, 73
- Natarajan, P., et al. 2005, *MNRAS*, 364, L8
- Nava, L., et al. 2008, *MNRAS*, 391, 639
- Norris, J. P., et al. 2000, *ApJ*, 534, 248
- Norris, J. P., Marani, G. F., & Bonnell J. T. 2000, *ApJ*, 534, 248
- Nysewander, M., Fructer, A. S., & Peér, A. 2009, *ApJ*, 701, 824
- Pelangeon, A., et al. 2008, *A&A*, 491, 157
- Perley, D. A., et al. 2007, GCN #6850?
- Perley, D. A., et al. 2008a, GCN #7962
- Perley, D. A., et al. 2008b, GCN #7889
- Perley, D. A., et al. 2009a, *AJ Accepted*, arXiv:0905.0001
- Perley, D. A., et al. 2009b, (in prep.)
- Petrosian, V. 1993, *ApJ*, 402, L33
- Petrosian, V. et al. 2009, arXiv:0909.5051
- Petrosian, V., & Lee, T. T. 1996, *ApJ*, 467, L29
- Piran, T., *ApJ*, 389, L45
- Piran, T., *Phys. Rep.*, 314, 575
- Porciani, C. & Madau, P. 2001, *ApJ*, 548, 522
- Preger, B., et al. 2001, in *Proc. Second Rome Workshop: Gamma-ray Bursts in the Afterglow Era*, ed. E. Costa, F. Frontera, & J. Hjorth (Berlin: Springer), 421
- Press, W. H., et al. 1992, *Numerical Recipes in C*, (2nd ed.; Cambridge: Cambridge Univ. Press)
- Prochaska, J. X., et al. 2007a, GCN #6698
- Prochaska, J. X., et al. 2007b, GCN #6864
- Prochaska, J. X., et al. 2008a, GCN #7397
- Prochaska, J. X., et al. 2008b, GCN #7849
- Prochaska, J. X., et al. 2008c, GCN #8083
- Racusin, J. L., et al. 2009, *ApJ*, 698, 43
- Rau, A., et al. 2009, GCN #9353
- Reichart, D. E., et al. 2001, *ApJ*, 552, 57
- Sakamoto, T., et al. 2005, *ApJ*, 629, 311
- Sakamoto, T., et al. 2007, *ApJ*, 669, 1115
- Sakamoto, T., et al. 2008, *ApJS*, 175, 179
- Salvaterra, R., & Chincarini, G. 2007, *ApJ*, 656, L49
- Salvaterra, R., et al. 2008, *MNRAS*, 385, 189
- Salvaterra, R., et al. 2009, *MNRAS*, 396, 299
- Salvaterra, R., et al. 2009, *Nature Submitted*, arXiv:0906.1578
- Savaglio, S. 2006, *New J. Phys.*, 8, 195
- Schaefer, B. E., et al. 2001, *ApJ*, 563, L123
- Schaeffer, B. E. 2003, *ApJ*, 583, L67
- Schmidt, M. 1968, *ApJ*, 151, 393
- Schmidt, M. 1999, *ApJ*, 532, L117
- Schmidt, M. 2001, *ApJ*, 552, 36
- Schmidt, M. 2009, *ApJ*, 700, 633
- Sethi, S. & Bhargavi, T. 2003, *A&A*, 376, 10
- Shahmoradi, A., & Nemiroff, R. J. 2009, *MNRAS Submitted*, arXiv:0904.1464
- Soderberg, A. M., et al. 2004, *Nature*, 430, 648
- Soderberg, A. M., et al. 2005, *ApJ*, 627, 877
- Stanek, K. Z., et al. 2003 *ApJ*, 591, L17
- Stanek, K. Z., et al. 2006, *Acta Astron.*, 56, 333
- Strohmer, T. E., et al. 1998, *ApJ*, 500, 873
- Tanvir, N. R., et al. 2009, *Nature Submitted*, arXiv:0906.1577
- Thoene, C. C., et al. 2007a, GCN #6499
- Thoene, C. C., et al. 2007b, GCN #6741
- Thoene, C. C., et al. 2008a, GCN #7587
- Thoene, C. C., et al. 2008b, GCN #7602
- Thoene, C. C., et al. 2009, GCN #9409
- Vreeswijk, P. M., et al. 2008a, GCN #7444
- Vreeswijk, P. M., et al. 2008b, GCN #7601
- Vreeswijk, P. M., et al. 2008d, GCN #8191
- Vreeswijk, P. M., et al. 2008d, GCN #8301
- Wiersama, K., et al. 2008a, GCN #7818
- Wiersema, K., et al. 2008b, GCN #7517
- Wiersema, K., et al. 2009, GCN #9673
- Wijers, R. M. A., et al. 1998, *MNRAS*, 294, L13
- Woosley, S. E., & Bloom, J. S. 2006, *ARA&A*, 44, 507
- Yonetoku, D., et al. 2004, *ApJ*, 609, 935
- Zhang, B., et al. 2008, *ApJ*, 703, 1696
- Zheng, W. K., et al. 2009, *RAA*, 9, 1103

APPENDIX

To rigorously accounts for measurement errors and for correlations present in the data, we characterize the GRB rate as a product of terms describing the intrinsic distributions in z , E_{iso} , $T_{r45,z}$, and $E_{\text{pk,obs}}$. Expanding the notation from Equation 3; Section 2, the the true, detector-independent event N differential rate is:

$$r_{\text{true}} = \frac{dN}{d \log[E_{\text{iso}}] d \log[E_{\text{pk}}] d \log[T_{r45,z}] dz} = P_{\text{corr}}(E_{\text{iso}}|E_{\text{pk}}, T_{r45,z}, z) P_E(E_{\text{pk}}) P_T(T_{r45,z}) \frac{r_0 \dot{\rho}(z) dV/dz}{(1+z)}, \quad (\text{A-1})$$

where P_{corr} is a luminosity function that allows for the potential dependence of E_{iso} on hardness, duration, and redshift.

We consider a regression model for P_{corr} :

$$P_{\text{corr}} = \int d \log[E_0] \frac{\phi_L(E_0)}{\sqrt{2\pi\sigma_L^2}} \exp(-0.5[\log(E_{\text{iso}}) - \log(E_0 E_{\text{pk}}^{\alpha_E} T_{r45,z}^{\alpha_T} (1+z)^{\alpha_z})]^2 / \sigma_L^2), \quad (\text{A-2})$$

where ϕ_L describes the normalization E_0 of the intrinsic correlation between luminosity, duration, hardness, and redshift. We can carry-out the integration, which can be regarded as a Gaussian smoothing of ϕ_L ,

$$P_{\text{corr}} = \tilde{\phi}_L(E_{\text{iso}}/E_{\text{pk}}^{\alpha_E}/T_{r45,z}^{\alpha_T}/(1+z)^{\alpha_z}/\sigma_L), \quad (\text{A-3})$$

without loss of generality.

In the case $\alpha_E = \alpha_T = \alpha_z = 0$, $\tilde{\phi}_L = \tilde{\phi}_L(E_{\text{iso}})$ is the luminosity function for E_{iso} smoothed by a Gaussian kernel of width σ_L . We think of $\tilde{\phi}_L$ as a luminosity function for the *effective* luminosity L (Equation 1). With parameters a , b , L_{cut} , and σ_L , we $\tilde{\phi}_L$ can take a wide variety of shapes: a sharply broken powerlaw ($\sigma_L \rightarrow 0$), a Gaussian ($a_L, -b_L \rightarrow \infty$), etc.

The Probability of Detection

In the derivation of the observed event rate $r_{\text{obs}} = \Theta(C - C_{\text{min}})r_{\text{true}}$ in Section 2, we write $\Theta(C - C_{\text{min}})$ as shorthand for the probability of detection of C counts: it is zero if $C < C_{\text{min}}$, one otherwise. In practice, the count rate cutoff is not sharp. More accurately, for a GRB reaching BAT with a given effective count rate $C_{\text{eff}} = C\sqrt{f_p/T_{r45}}$ (Section 2), we determine the probability of detection as:

$$\Theta(C - C_{\text{min}}) \Rightarrow P(\text{detect}|C_{\text{eff}}) = \frac{1}{2} + \frac{1}{2}\text{erf}\left(\frac{\log(C_{\text{eff}}/C_{\text{eff,min}})}{\sigma_{C_{\text{eff}}}\sqrt{2}}\right), \quad (\text{A-4})$$

where erf is the error function. This is the result of a convolution of $\Theta(C - C_{\text{min}})$ in Equation 4 with a log-Gaussian of width $\sigma_{C_{\text{eff}}}$. The convolution allows the count rate cutoff to be smooth.

In principle, just as faint GRBs with low C values are missing from the observed sample, some $C_{\text{eff,min}}$ are also missing. Our estimate of 0.24 ± 0.05 above will then be biased (see, e.g., Petrosian & Lee 1996). It is necessary, therefore, to fit for $C_{\text{eff,min}}$ and $\sigma_{C_{\text{eff}}}$. In practice, we find that $C_{\text{eff,min}}$ varies little (see, Table 1) and $\sigma_{C_{\text{eff}}}$ can be fixed to 0.1 dex without significantly affecting the other best-fit model parameters.

In the case of unknown partial coding fraction p_f , $P(\text{detect}|C_{\text{eff}})$ must be convolved with the log(p_f) distribution, which is well-described as an exponential with mean -0.23 . This situation arises in the calculation of the model normalization A in equation A-5. Here, we also require a prescription for determining the expected C_{eff} given intrinsic values of z , E_{iso} , E_{pk} , and T_{r45} . This connection between input (S_{bol} , $E_{\text{pk,obs}}$) and C is found by fitting a smooth curve to the observed data for all GRBs in the sample. We realized after the fact that these curves corresponds accurately to one derived from fixing a low energy (Band et al. 1993) model spectral index of -1.1 and a high energy index of -2.3 for all GRBs. This is in keeping with the prior assumptions (see Paper I) made in the spectral fitting. The scatter between the observed C and predicted C given this spectrum (for fixed values of S_{bol} and $E_{\text{pk,obs}}$) is less than 0.05 dex. Therefore, to the extent that other sources of error dominate (e.g., that in E_{pk}), it is acceptable in the current study to assume all Swift GRBs have the same (Band et al. 1993) model powerlaw spectral indices when normalizing the model in Equation A-5.

Model Fitting

To fit the model $r_{\text{obs}}(\vec{\theta})$ to the observed data D by finding the optimal parameters $\vec{\theta}$, we maximize the Poisson likelihood (e.g., Gregory 2005):

$$\mathcal{L}(D|\vec{\theta}) = A^N \prod_{i=0}^N r_i(\vec{\theta}) \exp[-A \int d\vec{\theta} r(\vec{\theta})], \quad (\text{A-5})$$

where r_i is the model evaluated for the i th GRB, and A is a normalization.

Each GRB has an associated range of acceptable values for E_{pk} , E_{iso} , and T_{r45} (Tables 3 & 4), and we average each r_i over these ranges. As discussed in Paper I, the spectral fitting returns highly correlated values for E_{pk} and E_{iso} , and this correlation is taken account via Monte Carlo integration as described in Paper I. The integration of $r(\vec{\theta})$ in the exponential in Equation A-5 for a given set of parameters $\vec{\theta}$ is independent of the data D and is carried out numerically. In the case of fitting GRBs without measured redshift (see Section 2.6), we must also integrate over the unknown z . The redshift integration is carried out over the interval $z = (0.2, \infty)$ to match the selected sample range (Section 2). In practice, the above integrations can be carried out rapidly ($\Delta t \approx 100\text{ms}$ for a given $\vec{\theta}$ on a desktop PC), and we utilize Markov Chain Monte Carlo techniques (Section 2.6) to stochastically explore the allowed parameter space.

Fitting is accomplished by maximizing Equation A-5 using Markov Chain Monte Carlo (MCMC) in python with PyMC¹¹. An MCMC method is preferred (relative, e.g., to direct maximization of Equation A-5) due to the high dimensionality of the fitting problem (17 model parameters) and the natural tendency to find local maxima rather than the global maximum. Moreover, MCMC methods return joint confidence regions on all parameters directly, without requiring that these distributions be tabulated in a computationally intensive way apart from the fitting.

Due to strong covariance among several model parameters (see below), we utilize the ‘‘Adaptive Metropolis’’ algorithm in PyMC to efficiently draw from the data posterior distribution. This algorithm employs an estimate of the posterior covariance matrix — based on the observed sample correlation matrix calculated after every 10^3 draws — to randomly walk through the parameter space. The presence of covariance in the Gaussian sampling distribution allows for a high acceptance rate for the draws. A scale factor is applied to the covariance matrix for sampling, and this is varied so that the acceptance rate approaches a target of 30%. (Higher rates correspond to insufficient randomness in

¹¹ <http://code.google.com/p/pymc>

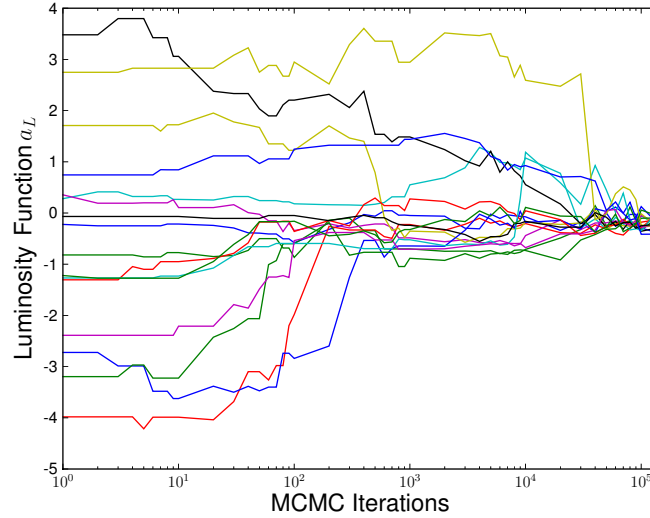


FIG. 12.— Uniqueness of the solution as demonstrated by the convergence of 16 MCMC chains, started from random positions in the parameter space, shown here for the luminosity function index a_L . Each chain converges to $a_L = -0.22$ and to the other parameters (not shown) in Table 1 (left) within 10^5 iterations. A logarithmic sampling of each chain is plotted for ease of viewing.

the sampling and failure to adequately explore the parameter space.) While the resulting chain is not strictly speaking Markov, it is ergodic. We refer the interested reader to the PyMC user guide¹² for more details.

We have initialized 16 chains randomly in the parameters space (Figure 12) and verified convergence to the values presented in Table 1. Convergence typically requires of order 2×10^4 iterations of each chain. After convergence (“burn in”) we record one out of every ten successive iterations until a total of 10^4 samples are acquired. This process of “thinning” the chain (e.g., Gelman et al. 2004) mitigates against sample to sample correlation. Best fit parameters and 90% confidence error bars are reported in Table 1.

¹² <http://pymc.googlecode.com/files/UserGuide2.0.pdf>

TABLE 3 BAT Trigger Statistics and Durations

GRB	Trigger Time (UTC)	Burst Region [s]	T_{90} [s]	T_{50} [s]	T_{r45} [s]	Rate _p /Cts [1/s]	$dt_{S/N}$ [s]	S/N
070517	11:20:58.39	0.255 → 7.745	6.2 ± 0.4	3.4 ± 0.6	1.5 ± 0.2	0.3 ± 0.1	6.86	8.7
070518	14:26:21.20	-0.650 → 5.650	5.3 ± 0.3	2.9 ± 0.4	1.2 ± 0.1	0.5 ± 0.2	5.94	10.1
070520A	13:05:10.03	25.565 → 61.205	31 ± 4	12 ± 4	5.3 ± 0.9	0.06 ± 0.05	16.83	7.5
070520B	17:44:53.26	-5.175 → 31.185	31 ± 2	15 ± 2	10 ± 1	0.05 ± 0.02	16.16	8.5
070521	06:51:10.86	-17.245 → 594.555	560 ± 10	16.8 ± 0.6	10.6 ± 0.6	0.074 ± 0.005	23.23	118.6
070529	12:48:28.34	0.595 → 121.965	112 ± 4	60 ± 4	23 ± 2	0.024 ± 0.006	121.37	13.5
070531	02:10:17.52	-2.920 → 41.080	37 ± 4	15 ± 4	6.6 ± 0.7	0.06 ± 0.03	20.20	14.4
070610	20:52:26.14	-0.490 → 10.010	8 ± 1	3.2 ± 0.6	1.6 ± 0.2	0.2 ± 0.1	5.58	12.7
070611	01:57:13.89	-4.515 → 8.225	11.3 ± 0.7	5 ± 1	2.6 ± 0.3	0.13 ± 0.09	10.53	10.4
070612A	02:38:45.98	-10.415 → 282.265	255 ± 5	182 ± 5	62 ± 3	0.010 ± 0.001	260.16	24.9
070612B	06:21:17.79	-9.250 → 11.710	16 ± 1	6.1 ± 0.7	4.3 ± 0.3	0.11 ± 0.03	13.76	24.2
070616	16:29:33.97	-18.530 → 710.110	440 ± 15	222 ± 5	135 ± 2	0.0070 ± 0.0002	396.00	149.2
070621	23:17:39.85	-10.220 → 40.180	36 ± 1	18.5 ± 0.6	13.0 ± 0.5	0.043 ± 0.008	41.58	48.8
070628	14:41:02.84	-0.855 → 17.215	13.3 ± 0.6	5.6 ± 0.2	4.4 ± 0.2	0.12 ± 0.02	11.57	50.5
070704	20:05:57.93	-58.265 → 388.885	385 ± 7	80 ± 13	31 ± 1	0.024 ± 0.002	33.00	74.2
070714A	03:20:30.61	0.912 → 4.292	2.6 ± 0.4	0.96 ± 0.10	0.62 ± 0.05	0.8 ± 0.3	1.52	21.5
070714B	04:59:29.62	0.150 → 66.670	64 ± 2	37 ± 5	1.4 ± 0.2	0.8 ± 0.1	2.78	35.8
070721A	10:01:08.00	-10.720 → -6.920	3.4 ± 0.3	1.8 ± 0.5	0.6 ± 0.1	0.4 ± 0.4	1.80	6.9
070721B	10:33:48.00	-9.230 → 358.170	330 ± 10	270 ± 12	17 ± 1	0.03 ± 0.01	22.44	26.8
070724A	10:53:50.21	0.995 → 1.725	0.6 ± 0.1	0.25 ± 0.05	0.11 ± 0.02	3 ± 1	0.49	8.6
070729	00:25:53.91	0.980 → 2.320	1.0 ± 0.1	0.58 ± 0.08	0.30 ± 0.04	1.2 ± 0.8	1.14	9.7
070731	09:33:24.00	-0.440 → 2.480	2.6 ± 0.2	1.8 ± 0.5	0.52 ± 0.07	0.8 ± 0.3	1.32	10.1
070802	07:07:25.87	5.990 → 23.270	15 ± 1	8 ± 1	3.5 ± 0.4	0.09 ± 0.05	15.20	7.3
070805	19:55:45.44	0.810 → 25.410	22.5 ± 0.7	14 ± 1	6.9 ± 0.7	0.07 ± 0.02	5.70	6.9
070808	18:28:00.54	-0.480 → 68.240	57 ± 8	20 ± 3	5.3 ± 0.4	0.11 ± 0.03	13.12	24.3
070809	19:22:17.37	1.180 → 2.040	0.76 ± 0.05	0.46 ± 0.05	0.26 ± 0.03	1.3 ± 0.8	0.70	7.1
070810A	02:11:52.41	-1.430 → 9.210	7.7 ± 0.7	3.4 ± 0.2	2.5 ± 0.2	0.17 ± 0.06	6.96	24.6
070810B	15:19:17.85	1.165 → 2.245	0.8 ± 0.5	0.3 ± 0.4	0.06 ± 0.02	8 ± 3	0.15	7.5
070911	05:57:44.00	-80.910 → 181.050	177 ± 4	68 ± 1	40 ± 1	0.0216 ± 0.0009	116.82	148.6
070913	00:36:43.00	-0.480 → 3.680	3.2 ± 0.4	1.4 ± 0.5	0.8 ± 0.1	0.6 ± 0.3	3.56	10.8
070917	07:33:56.00	1.600 → 13.840	7.4 ± 0.6	2.4 ± 0.1	1.52 ± 0.05	0.36 ± 0.03	4.48	82.0
070920A	04:00:13.00	14.200 → 79.600	57 ± 2	36 ± 6	14 ± 1	0.03 ± 0.02	61.20	12.9
070920B	21:04:32.38	-13.575 → 13.725	21.6 ± 1.0	8.8 ± 0.7	7.1 ± 0.4	0.06 ± 0.02	22.89	31.3
070923	19:15:23.68	1.235 → 1.495	0.18 ± 0.03	0.05 ± 0.04	0.030 ± 0.005	18 ± 3	0.06	10.8
071001	16:31:48.07	-12.620 → 64.280	66 ± 3	46 ± 1	7.8 ± 0.7	0.06 ± 0.02	9.50	20.1
071003	07:40:55.01	-10.310 → 168.970	148 ± 1	19 ± 1	10.3 ± 0.5	0.067 ± 0.008	24.24	79.7
071008	21:55:56.76	-5.010 → 10.110	12 ± 1	4.9 ± 0.7	2.9 ± 0.4	0.11 ± 0.06	8.12	12.5
071010A	03:41:12.85	-8.795 → 15.705	22 ± 2	9 ± 3	1.8 ± 0.4	0.1 ± 0.1	24.36	7.5
071010B	20:45:47.98	-27.980 → 33.340	35 ± 1	6.0 ± 0.2	4.7 ± 0.1	0.107 ± 0.007	11.64	136.3
071011	12:40:13.00	-11.160 → 96.280	87 ± 8	44 ± 1	18 ± 1	0.046 ± 0.006	67.32	28.7
071013	12:09:19.05	-5.635 → 32.065	34 ± 5	12 ± 5	4.9 ± 0.9	0.06 ± 0.04	29.29	8.7
071018	08:37:41.70	118.800 → 448.800	290 ± 20	160 ± 28	39 ± 4	0.006 ± 0.004	304.00	7.7
071020	07:02:26.94	-2.020 → 9.460	4.4 ± 0.4	2.04 ± 0.04	1.36 ± 0.03	0.38 ± 0.05	3.64	100.3
071021	09:41:33.69	-13.410 → 214.790	200 ± 29	54 ± 8	18 ± 1	0.026 ± 0.010	28.28	17.7
071025	04:08:53.68	24.175 → 280.485	161 ± 8	49 ± 1	39 ± 1	0.014 ± 0.002	70.29	86.0
071028A	17:41:01.67	11.015 → 56.155	36 ± 5	17 ± 2	7.4 ± 1.0	0.05 ± 0.03	37.00	10.9
071031	01:06:36.96	-11.505 → 208.145	190 ± 11	118 ± 8	34 ± 4	0.021 ± 0.005	200.55	15.9
071101	17:53:46.59	0.785 → 5.225	3.7 ± 0.8	1.7 ± 0.5	0.51 ± 0.10	0.5 ± 0.5	4.05	7.8
071112B	18:23:31.53	0.740 → 1.960	0.9 ± 0.2	0.2 ± 0.4	0.10 ± 0.03	4 ± 1	0.38	8.9
071117	14:50:06.91	0.810 → 15.210	6 ± 1	1.7 ± 0.1	1.28 ± 0.05	0.42 ± 0.06	3.76	76.4
071118	08:57:17.62	5.390 → 69.610	57 ± 6	31 ± 6	8 ± 1	0.03 ± 0.03	63.84	8.3
071122	01:23:25.62	-25.920 → 66.880	79 ± 8	44 ± 7	16 ± 2	0.02 ± 0.01	92.00	10.0
071129	00:03:55.00	-6.340 → 232.700	210 ± 11	150 ± 10	27 ± 2	0.017 ± 0.006	28.80	23.9
071227	20:13:47.04	0.890 → 3.710	2.2 ± 0.3	0.9 ± 0.2	0.50 ± 0.06	0.7 ± 0.4	2.42	13.8
080123	04:21:57.40	44.450 → 72.270	26 ± 4	11 ± 5	3.1 ± 0.8	0.13 ± 0.09	25.74	5.3
080129	06:06:45.46	-8.720 → 47.920	46 ± 4	24 ± 3	10 ± 1	0.03 ± 0.02	47.04	11.6
080205	07:55:51.75	-11.135 → 129.395	113 ± 4	86 ± 2	21 ± 1	0.032 ± 0.008	47.00	33.6
080207	21:30:21.44	13.250 → 347.590	310 ± 15	180 ± 52	70 ± 10	0.02 ± 0.06	169.36	61.9
080210	07:50:05.43	-13.995 → 49.425	44 ± 7	12 ± 1	8.8 ± 0.6	0.05 ± 0.01	21.63	36.6
080212	17:34:33.46	-63.680 → 111.120	132 ± 4	61 ± 7	35 ± 2	0.015 ± 0.005	150.48	24.7
080218A	20:08:42.00	-10.140 → 22.740	27 ± 4	13 ± 4	4.6 ± 0.7	0.07 ± 0.05	24.00	9.4
080218B	23:57:47.17	-0.475 → 7.715	6.3 ± 0.9	2.9 ± 0.6	1.4 ± 0.2	0.4 ± 0.2	5.94	11.1
080229A	17:04:59.53	-1.795 → 71.395	50 ± 2	11.7 ± 0.6	7.0 ± 0.2	0.112 ± 0.008	12.61	111.6

Continued on Next Page...

TABLE 3 – Continued

GRB	Trigger Time	Burst Region	T_{90}	T_{50}	T_{r45}	Rate _p /Cts	$dt_{S/N}$	S/N
080303	09:10:35.27	1.130 → 53.570	45 ± 3	17 ± 6	2.7 ± 0.3	0.15 ± 0.08	4.44	17.5
080307	11:23:30.81	-1.975 → 111.925	98 ± 8	40 ± 5	19 ± 2	0.020 ± 0.007	66.33	16.9
080310	08:37:58.64	-66.540 → 322.900	362 ± 6	251 ± 5	24 ± 1	0.025 ± 0.007	15.84	27.5
080319A	05:45:42.05	-7.355 → 50.365	46 ± 2	23 ± 1	13.3 ± 0.9	0.03 ± 0.01	38.22	23.9
080319B	06:12:49.25	-2.880 → 783.020	147 ± 4	27.3 ± 0.5	20.30 ± 0.10	0.0273 ± 0.0005	58.58	725.4
080319C	12:25:56.96	-0.280 → 53.120	33 ± 5	7.8 ± 0.4	5.0 ± 0.3	0.12 ± 0.02	12.36	60.5
080319D	17:05:09.00	-0.335 → 37.285	30 ± 5	17 ± 3	5.6 ± 1.0	0.04 ± 0.04	33.00	8.3
080320	04:37:38.46	-8.870 → 16.510	21 ± 3	8 ± 1	4.1 ± 0.5	0.10 ± 0.05	17.46	13.6
080325	04:09:17.33	-35.620 → 216.060	184 ± 9	77 ± 8	41 ± 4	0.010 ± 0.004	244.42	18.1
080328	08:03:04.58	-3.580 → 109.420	91.0 ± 0.5	67.0 ± 0.6	16.0 ± 0.3	0.049 ± 0.003	97.00	83.7
080330	03:41:16.87	1.080 → 70.680	66 ± 1	50 ± 30	4.0 ± 0.6	0.10 ± 0.05	9.60	13.4
080409	01:22:57.58	1.330 → 12.170	9.9 ± 0.2	8 ± 3	0.90 ± 0.09	0.5 ± 0.1	1.58	24.7
080411	21:15:32.58	-8.335 → 88.145	58.3 ± 0.8	25.5 ± 0.1	6.7 ± 0.1	0.112 ± 0.001	67.00	379.3
080413A	02:54:19.30	0.935 → 55.115	46.6 ± 0.2	15.8 ± 0.6	5.3 ± 0.2	0.120 ± 0.008	20.58	74.8
080413B	08:51:12.54	0.220 → 12.340	7.0 ± 0.7	1.7 ± 0.1	1.16 ± 0.05	0.41 ± 0.05	4.16	64.4
080426	13:23:22.94	1.510 → 3.850	1.7 ± 0.2	0.64 ± 0.08	0.34 ± 0.03	1.5 ± 0.3	1.28	28.1
080430	19:53:02.07	0.745 → 22.795	16 ± 1	5.4 ± 0.4	3.4 ± 0.1	0.14 ± 0.03	8.55	52.7
080503	12:26:13.42	1.395 → 243.945	180 ± 31	51 ± 6	27 ± 2	0.038 ± 0.006	63.63	34.5
080506	17:46:21.22	22.450 → 190.150	152 ± 4	100 ± 11	31 ± 2	0.012 ± 0.005	78.00	19.3
080515	06:01:13.00	-5.945 → 24.505	22 ± 2	9 ± 1	6.1 ± 0.5	0.06 ± 0.03	21.21	18.8
080516	00:17:07.03	1.655 → 9.485	6.8 ± 0.3	5.4 ± 0.2	1.0 ± 0.2	0.5 ± 0.2	7.20	11.9
080517	21:22:51.98	0.240 → 30.800	27 ± 4	11 ± 3	4.0 ± 0.6	0.12 ± 0.05	20.32	11.2
080520	22:20:24.77	1.355 → 5.045	3.0 ± 0.4	1.8 ± 0.3	0.51 ± 0.08	1.3 ± 0.6	3.18	8.3
080523	21:21:51.29	-8.595 → 61.995	55 ± 5	23 ± 2	13 ± 1	0.04 ± 0.01	38.61	21.6
080602	01:30:28.07	-21.485 → 71.195	85 ± 4	60 ± 1	7.0 ± 0.5	0.08 ± 0.02	7.70	39.5
080603B	19:38:13.28	0.510 → 72.050	59.5 ± 0.8	45.6 ± 0.7	6.2 ± 0.3	0.11 ± 0.01	13.44	70.0
080604	07:27:01.15	-27.345 → 111.855	125 ± 8	51 ± 8	27 ± 2	0.020 ± 0.006	87.00	16.1
080607	06:07:27.00	-6.030 → 206.410	84 ± 1	25.4 ± 0.9	7.5 ± 0.2	0.076 ± 0.004	93.06	123.0
080605	23:47:57.85	-6.065 → 31.555	19.6 ± 0.5	7.2 ± 0.2	4.8 ± 0.1	0.134 ± 0.006	19.76	157.5
080613B	11:12:37.96	-4.125 → 153.285	83 ± 8	27 ± 1	15.9 ± 0.6	0.047 ± 0.003	53.00	94.4
080623	10:25:28.44	0.210 → 19.710	16 ± 1	6.5 ± 0.4	2.9 ± 0.3	0.19 ± 0.05	9.20	21.5
080701	10:13:37.63	-1.405 → 11.245	9.4 ± 0.8	3.3 ± 0.4	2.3 ± 0.2	0.22 ± 0.08	5.55	26.7
080702A	11:50:43.68	1.865 → 2.375	0.44 ± 0.07	0.21 ± 0.06	0.08 ± 0.02	4 ± 2	0.37	6.9
080703	19:00:13.59	-0.670 → 5.090	4.2 ± 0.6	1.8 ± 0.4	0.8 ± 0.1	0.4 ± 0.2	4.76	10.8
080707	08:27:53.68	-0.305 → 33.245	30.3 ± 0.7	24.1 ± 0.6	3.3 ± 0.3	0.10 ± 0.06	5.45	17.2
080710	07:13:10.79	-97.615 → 68.435	140 ± 16	73 ± 8	23 ± 3	0.033 ± 0.009	135.00	12.6
080714	17:52:56.64	-3.090 → 49.210	34 ± 3	10 ± 1	4.7 ± 0.3	0.13 ± 0.01	17.10	44.9
080721	10:25:16.97	-9.665 → 83.945	30 ± 3	6.8 ± 0.3	4.5 ± 0.3	0.14 ± 0.03	17.82	37.2
080723A	04:19:24.39	0.345 → 33.405	25 ± 4	13 ± 1	3.8 ± 0.6	0.16 ± 0.04	20.52	14.0
080725	10:26:14.63	-103.710 → 54.770	130 ± 7	15 ± 1	11.2 ± 0.9	0.043 ± 0.007	27.16	46.1
080727A	05:57:39.36	1.790 → 10.130	6 ± 1	2.6 ± 0.7	0.9 ± 0.2	0.2 ± 0.3	5.28	7.9
080727B	08:13:24.95	0.300 → 75.900	20 ± 18	6.6 ± 0.1	2.20 ± 0.10	0.27 ± 0.03	9.70	81.4
080727C	23:07:35.39	-2.650 → 163.430	100 ± 9	28 ± 1	18.2 ± 0.7	0.034 ± 0.003	54.72	76.2
080802	15:12:21.07	-28.890 → 176.070	170 ± 14	81 ± 9	30 ± 3	0.019 ± 0.005	110.88	18.0
080804	23:20:14.66	-0.090 → 107.550	60 ± 14	13 ± 2	7.9 ± 0.6	0.06 ± 0.02	17.10	31.1
080805	07:41:34.73	-3.990 → 142.890	110 ± 14	39 ± 4	20 ± 1	0.028 ± 0.004	48.48	49.7
080810	13:10:12.28	-19.495 → 466.145	453 ± 8	90 ± 13	31 ± 2	0.024 ± 0.002	57.00	57.9
080822B	21:02:52.96	26.540 → 72.540	39 ± 3	29 ± 8	6 ± 1	0.05 ± 0.04	42.00	4.2
080903	01:12:23.30	-10.645 → 81.425	69 ± 5	25 ± 2	15.5 ± 1.0	0.030 ± 0.007	32.01	37.5
080905A	11:58:54.97	2.080 → 3.320	1.04 ± 0.05	0.86 ± 0.05	0.18 ± 0.03	4 ± 1	1.16	11.4
080905B	16:55:45.40	-0.055 → 130.185	104 ± 7	78 ± 2	13 ± 1	0.05 ± 0.02	37.74	22.8
080906	13:33:16.34	-84.920 → 150.040	160 ± 11	44 ± 2	30 ± 1	0.017 ± 0.003	88.00	47.2
080913	06:46:54.12	-2.485 → 7.595	8.2 ± 0.4	4.1 ± 0.8	2.2 ± 0.2	0.17 ± 0.07	9.00	16.7
080915A	00:02:49.95	0.675 → 13.545	10 ± 1	5 ± 1	2.0 ± 0.3	0.2 ± 0.1	10.23	9.0
080915B	15:53:35.14	1.470 → 6.790	3.6 ± 0.4	1.04 ± 0.06	0.84 ± 0.03	0.6 ± 0.1	2.02	53.3
080916A	09:45:20.61	-0.555 → 101.195	63 ± 5	23.7 ± 0.9	13.3 ± 0.4	0.047 ± 0.004	37.00	89.3
080916B	14:44:47.32	-1.875 → 37.815	34 ± 3	15 ± 2	6.1 ± 0.8	0.05 ± 0.03	20.16	11.5
080919	00:05:13.05	1.780 → 3.420	1.4 ± 0.1	0.50 ± 0.09	0.30 ± 0.04	1.1 ± 0.6	1.60	11.5
080928	15:01:32.86	-11.890 → 320.050	280 ± 19	120 ± 10	23 ± 1	0.055 ± 0.008	14.14	39.8
081007	05:23:52.74	0.935 → 8.735	5.6 ± 0.4	2.7 ± 0.3	1.6 ± 0.1	0.3 ± 0.1	5.70	19.6
081008	19:58:09.38	-63.615 → 223.285	200 ± 18	112 ± 1	32 ± 1	0.020 ± 0.002	152.51	50.7
081011	00:28:50.46	0.015 → 21.725	19 ± 2	8 ± 2	2.9 ± 0.5	0.13 ± 0.06	12.61	10.0
081012	13:10:23.90	-21.300 → 19.900	32 ± 3	10 ± 1	6.0 ± 0.7	0.07 ± 0.04	17.60	16.3
081016B	19:47:14.51	2.160 → 3.980	1.6 ± 0.2	0.8 ± 0.2	0.32 ± 0.05	0.7 ± 0.7	1.78	7.8
081017	23:38:12.81	-32.085 → 258.615	250 ± 14	130 ± 16	31 ± 3	0.005 ± 0.006	63.90	8.1

Continued on Next Page...

TABLE 3 – Continued

GRB	Trigger Time	Burst Region	T_{90}	T_{50}	T_{r45}	Rate _p /Cts	dt _{S/N}	S/N
081022	14:23:48.80	-6.750 → 189.050	150 ± 13	61 ± 5	43 ± 2	0.011 ± 0.003	112.20	28.3
081024A	05:53:08.86	0.490 → 2.550	1.86 ± 0.08	0.6 ± 0.2	0.26 ± 0.04	2.3 ± 0.6	0.72	14.5
081028	00:25:00.79	32.795 → 384.335	280 ± 15	135 ± 4	78 ± 3	0.0077 ± 0.0010	214.83	42.0
081029	01:43:56.78	-48.430 → 156.770	170 ± 14	74 ± 7	49 ± 4	0.007 ± 0.004	190.00	16.0
081101	11:46:31.97	2.180 → 2.520	0.22 ± 0.05	0.12 ± 0.02	0.08 ± 0.01	6 ± 1	0.20	13.1
081102	17:44:39.52	-20.995 → 64.955	63 ± 7	19 ± 2	13 ± 1	0.042 ± 0.007	44.55	25.4
081104	09:34:42.46	-3.060 → 47.980	41 ± 1	20 ± 1	13 ± 1	0.04 ± 0.01	45.76	22.4
081109A	07:02:06.61	-25.940 → 78.640	70 ± 3	24 ± 1	17.2 ± 0.7	0.028 ± 0.004	43.26	58.7
081109B	13:47:16.75	33.750 → 134.750	95 ± 5	70 ± 20	9 ± 2	0.05 ± 0.04	101.00	4.1
081118	14:56:36.73	11.895 → 103.195	67 ± 8	29 ± 2	18 ± 1	0.020 ± 0.008	54.45	19.8
081121	20:35:32.85	-6.455 → 17.485	19 ± 1	9.9 ± 0.9	5.5 ± 0.4	0.14 ± 0.04	19.19	24.4
081126	21:34:10.28	-22.905 → 59.245	60 ± 2	31.6 ± 0.2	6.6 ± 0.3	0.09 ± 0.01	5.95	52.9
081127	07:05:08.00	-10.495 → 19.865	22 ± 3	11 ± 1	4.8 ± 0.7	0.06 ± 0.04	23.92	10.3
081128	17:18:44.70	-64.080 → 85.680	108 ± 5	33 ± 3	24 ± 1	0.027 ± 0.006	48.96	36.2
081203A	13:57:11.57	-66.900 → 400.320	250 ± 44	46 ± 4	31 ± 1	0.027 ± 0.004	78.78	80.3
081210	20:19:34.21	-13.565 → 156.935	151 ± 3	20 ± 17	12 ± 1	0.10 ± 0.01	31.62	35.9
081211A	11:48:10.69	0.965 → 6.705	4.8 ± 0.8	2.0 ± 0.6	1.0 ± 0.2	0.3 ± 0.3	5.32	7.5
081221	16:21:11.84	1.765 → 144.985	34 ± 1	9.2 ± 0.1	8.0 ± 0.1	0.069 ± 0.002	20.58	278.7
081222	04:53:59.97	0.430 → 66.430	33 ± 2	5.8 ± 0.3	4.20 ± 0.09	0.121 ± 0.006	11.40	147.6
081226A	01:03:37.37	2.260 → 2.980	0.6 ± 0.1	0.24 ± 0.07	0.16 ± 0.03	3 ± 1	0.50	10.2
081228	01:17:40.75	1.780 → 6.220	3.8 ± 0.7	1.3 ± 0.4	0.48 ± 0.08	1.0 ± 0.4	2.22	9.7
081230	20:36:12.62	5.990 → 69.070	55 ± 2	20 ± 2	12 ± 1	0.05 ± 0.01	37.24	22.2
090102	02:55:45.86	-12.865 → 32.675	31 ± 1	13 ± 1	8.3 ± 0.5	0.06 ± 0.01	33.66	35.5
090107A	04:48:17.00	2.125 → 19.375	13 ± 1	10.8 ± 0.5	2.0 ± 0.4	0.28 ± 0.09	1.35	9.8
090111	23:58:34.70	-6.665 → 29.515	30 ± 3	14.6 ± 0.7	7.3 ± 0.6	0.06 ± 0.02	27.00	20.0
090113	18:40:52.17	2.080 → 12.680	8.8 ± 0.2	5.8 ± 0.6	2.0 ± 0.1	0.35 ± 0.05	10.30	32.3
090123	07:52:09.32	-48.285 → 122.405	142 ± 8	41 ± 7	25 ± 2	0.031 ± 0.006	167.31	24.6
090129	21:07:28.28	2.455 → 30.535	18 ± 1	7.3 ± 0.3	4.6 ± 0.2	0.12 ± 0.01	10.40	68.7
090201	17:47:15.73	-19.940 → 127.980	89 ± 2	42 ± 1	16.3 ± 0.8	0.036 ± 0.002	86.00	88.6
090205	23:03:27.82	-2.780 → 11.380	11 ± 1	5.2 ± 0.9	2.6 ± 0.3	0.11 ± 0.06	12.24	13.0
090301	06:56:08.14	-14.925 → 86.345	43 ± 2	20.1 ± 0.3	10.7 ± 0.3	0.071 ± 0.003	41.00	179.8
090305	05:20:04.03	3.540 → 4.460	0.7 ± 0.2	0.28 ± 0.09	0.14 ± 0.03	4 ± 1	0.46	9.6
090307	03:46:50.87	-4.530 → 21.870	22 ± 3	12 ± 3	3.1 ± 0.7	0.05 ± 0.09	24.00	6.0
090308	18:01:36.44	-224.545 → 55.175	264 ± 5	230 ± 55	10 ± 2	0.02 ± 0.02	29.16	9.0
090309	23:29:26.26	2.845 → 5.965	2.5 ± 0.3	1.1 ± 0.2	0.54 ± 0.08	0.6 ± 0.4	2.94	9.6
090313	09:06:40.42	-27.450 → 86.290	90 ± 11	45 ± 6	23 ± 2	0.02 ± 0.01	92.12	12.4
090401A	00:01:12.37	-10.330 → 172.910	117 ± 9	25.2 ± 0.7	13.0 ± 0.5	0.080 ± 0.006	35.64	109.6
090401B	08:35:37.86	3.180 → 357.299	230 ± 28	10 ± 2	3.1 ± 0.1	0.209 ± 0.007	12.00	156.5
090404	15:56:43.44	-39.830 → 97.810	86 ± 6	40 ± 1	21 ± 1	0.037 ± 0.002	74.00	61.7
090407	10:28:38.63	-10.530 → 144.670	148 ± 1	100 ± 66	6 ± 1	0.06 ± 0.03	16.32	13.5
090408	15:02:24.35	41.150 → 70.150	28 ± 4	14 ± 5	6 ± 1	0.08 ± 0.05	28.00	3.5
090410	16:58:05.85	-46.975 → 157.525	167 ± 2	100 ± 1	26.3 ± 1.0	0.034 ± 0.005	25.25	67.4
090417A	13:17:36.79	3.595 → 3.755	0.12 ± 0.02	0.05 ± 0.02	0.040 ± 0.010	14 ± 5	0.14	8.4
090417B	15:20:16.33	322.845 → 611.945	252 ± 8	142 ± 8	88 ± 5	0.004 ± 0.002	276.85	25.1
090418	11:07:53.22	-6.705 → 68.005	58 ± 1	33 ± 2	17.1 ± 0.7	0.034 ± 0.005	30.69	52.4
090419	13:43:44.32	-0.750 → 472.590	433 ± 8	260 ± 28	80 ± 6	0.006 ± 0.003	198.72	14.3
090422	03:35:29.60	3.330 → 61.550	60 ± 15	50 ± 25	1.2 ± 0.2	0.5 ± 0.1	1.14	16.1
090423	07:55:32.34	1.580 → 18.740	12.4 ± 1.0	5.4 ± 0.3	3.8 ± 0.2	0.15 ± 0.02	12.48	31.3
090424	14:12:22.33	1.960 → 107.740	50.3 ± 0.9	3.42 ± 0.04	1.98 ± 0.05	0.27 ± 0.02	9.24	131.7
090426	12:49:00.21	3.520 → 5.160	1.3 ± 0.1	0.48 ± 0.09	0.32 ± 0.04	1.4 ± 0.5	1.38	13.0
090429A	04:53:52.00	-8.625 → 26.125	28 ± 1	12 ± 1	7.8 ± 0.6	0.06 ± 0.02	25.50	20.4
090429B	05:30:16.36	-0.885 → 6.665	5.8 ± 0.5	2.6 ± 0.2	1.5 ± 0.1	0.3 ± 0.1	4.20	22.1
090509	05:10:16.59	-0.020 → 309.380	293 ± 4	253 ± 9	16 ± 1	0.03 ± 0.01	27.04	17.1
090510	00:23:13.48	3.310 → 4.270	0.5 ± 0.1	0.26 ± 0.03	0.12 ± 0.02	5 ± 1	0.62	14.9
090515	04:45:22.52	3.735 → 3.875	0.07 ± 0.04	0.020 ± 0.010	0.020 ± 0.007	41 ± 8	0.05	11.1
090516	08:28:03.77	-16.590 → 329.490	230 ± 15	81 ± 4	37 ± 3	0.016 ± 0.003	336.00	24.0
090518	01:54:57.27	1.010 → 52.570	50 ± 11	5 ± 8	1.7 ± 0.3	0.30 ± 0.06	3.64	24.1
090519	21:09:09.42	-11.255 → 89.015	82 ± 9	39 ± 8	14 ± 1	0.03 ± 0.01	37.00	15.2
090529	14:12:48.21	-45.525 → 45.325	80 ± 5	36 ± 4	19 ± 2	0.02 ± 0.02	79.00	17.7
090530	03:18:31.38	3.180 → 52.100	41 ± 1	25 ± 7	2.6 ± 0.3	0.24 ± 0.06	4.08	23.7
090531A	01:45:30.38	-22.030 → 56.870	46 ± 8	15 ± 1	11.7 ± 0.8	0.051 ± 0.008	29.40	32.8
090531B	18:36:09.17	3.860 → 62.340	55.5 ± 0.6	41 ± 2	2.4 ± 0.3	0.3 ± 0.1	1.04	20.1
090607	05:30:30.40	3.695 → 6.905	2.5 ± 0.2	1.9 ± 0.1	0.48 ± 0.06	1.1 ± 0.5	2.55	11.3
090618	08:28:42.85	-11.630 → 318.130	115.2 ± 0.7	30.2 ± 0.6	23 ± 1	0.0257 ± 0.0003	144.00	719.8
090621B	22:07:38.64	3.770 → 4.110	0.20 ± 0.05	0.08 ± 0.02	0.060 ± 0.010	10 ± 3	0.18	13.1

Continued on Next Page...

TABLE 3 – Continued

GRB	Trigger Time	Burst Region	T_{90}	T_{50}	T_{r45}	Rate _p /Cts	$dt_{S/N}$	S/N
090628	21:20:25.02	-21.395 → 11.455	28 ± 2	11 ± 2	2.9 ± 0.3	0.14 ± 0.09	4.45	18.2
090708	03:38:28.26	1.780 → 19.420	14 ± 1	6 ± 1	2.8 ± 0.3	0.09 ± 0.07	12.00	13.2
090709A	07:38:47.59	-66.665 → 509.035	300 ± 105	38.0 ± 0.9	28.5 ± 0.8	0.024 ± 0.001	95.95	251.6
090709B	15:07:55.87	-0.820 → 38.080	31 ± 2	13 ± 4	4.3 ± 0.4	0.10 ± 0.05	10.40	17.7
090712	03:51:18.00	-97.190 → 115.470	170 ± 16	44 ± 4	32 ± 2	0.014 ± 0.006	68.20	29.9
090715A	17:25:52.00	3.910 → 5.890	0.9 ± 0.5	0.26 ± 0.10	0.18 ± 0.03	3 ± 1	0.68	15.2
090715B	21:03:27.63	-9.065 → 299.815	268 ± 7	64 ± 1	15.3 ± 1.0	0.046 ± 0.005	13.00	84.9
090726	22:42:40.75	-15.965 → 42.355	51 ± 1	19 ± 3	9.2 ± 0.9	0.06 ± 0.02	27.00	17.2
090727	22:42:31.02	0.570 → 322.410	301 ± 6	252 ± 7	16 ± 1	0.02 ± 0.01	16.38	12.3
090728	14:45:58.96	-4.550 → 37.830	33 ± 5	14 ± 2	7.0 ± 0.8	0.06 ± 0.03	25.74	15.0
090807	15:00:40.02	-14.705 → 162.965	152 ± 6	83 ± 9	42 ± 3	0.013 ± 0.005	161.37	21.3
090809	17:31:27.50	2.365 → 201.585	190 ± 30	130 ± 62	3.4 ± 0.7	0.10 ± 0.06	6.65	11.8
090812	06:02:21.89	-85.445 → 136.005	100 ± 26	26 ± 1	18.5 ± 0.7	0.054 ± 0.004	44.29	78.6
090813	04:10:56.15	1.555 → 12.355	7.9 ± 0.4	6.1 ± 0.1	1.0 ± 0.1	0.63 ± 0.10	8.28	28.0

Notes: Detailed descriptions of the above quantities can be found in Paper I.

TABLE 4 BAT Spectral Fits

GRB	$-\alpha$	$-\beta$	$E_{\text{pk,obs}}^{\text{freq.}}$ [keV]	S_{15-350} [$10^{-6} \frac{\text{erg}}{\text{cm}^2}$]	$\chi^2/\nu^{(\text{model})}$	$E_{\text{pk,obs}}$ [keV]	N_{iso} or n_{bol} [$10^{59} \gamma$ or $10^2 \frac{\gamma}{\text{cm}^2}$]	E_{iso} or S_{bol} [10^{52}erg or $10^{-6} \frac{\text{erg}}{\text{cm}^2}$]	$z^{(\text{ref})}$
070517	1.7 ± 0.2	...	>45	0.37 ± 0.06	47.9/56 ¹	67^{+178}_{-35}	$0.13^{+0.12}_{-0.05}$	$0.34^{+0.32}_{-0.07}$...
070518	...	2.1 ± 0.3	<42	0.21 ± 0.03	66.1/56 ¹	35 ± 33	$0.3^{+1.9}_{-0.1}$	$0.09^{+0.15}_{-0.01}$	1.16 ¹
070520A	0^{+1}_{-2}	...	70^{+180}_{-20}	$0.33^{+0.09}_{-0.06}$	52.8/55 ²	74^{+243}_{-35}	$0.14^{+0.14}_{-0.05}$	$0.5^{+0.6}_{-0.1}$...
070520B	1.1 ± 0.2	...	>110	2.5 ± 0.4	54.8/56 ¹	370^{+620}_{-220}	$0.32^{+0.13}_{-0.08}$	4^{+5}_{-2}	...
070521	1.35 ± 0.07	...	>152	16.4 ± 0.7	52.7/56 ¹	300^{+550}_{-160}	$3.5^{+0.9}_{-0.6}$	23^{+20}_{-8}	...
070529	1.3 ± 0.2	...	>124	5.2 ± 0.5	44.3/56 ¹	250^{+620}_{-190}	5^{+4}_{-2}	9^{+9}_{-3}	2.4996 ²
070531	1.4 ± 0.2	...	>82	2.0 ± 0.3	57.8/56 ¹	165^{+499}_{-73}	$0.37^{+0.26}_{-0.09}$	$2.1^{+3.0}_{-0.6}$...
070610	1.8 ± 0.3	0.41 ± 0.08	73.3/56 ¹	74^{+424}_{-72}	$0.18^{+0.69}_{-0.05}$	$0.43^{+0.67}_{-0.05}$...
070611	0^{+1}_{-2}	...	50^{+50}_{-10}	$0.34^{+0.07}_{-0.05}$	69.6/55 ²	67^{+113}_{-26}	$0.7^{+1.1}_{-0.3}$	$0.5^{+0.4}_{-0.1}$	2.04 ³
070612A	1.58 ± 0.10	...	>118	17.1 ± 0.9	47.4/56 ¹	149^{+472}_{-59}	4^{+3}_{-1}	$2.0^{+1.8}_{-0.4}$	0.617 ⁴
070612B	0.8 ± 0.6	...	80^{+60}_{-20}	$2.1^{+0.3}_{-0.2}$	53.9/55 ²	90^{+65}_{-38}	$0.7^{+0.5}_{-0.2}$	$2.7^{+1.1}_{-0.4}$...
070616	1.3 ± 0.2	...	160^{+220}_{-40}	29 ± 1	55.1/55 ²	149^{+132}_{-13}	11^{+4}_{-2}	39^{+14}_{-6}	...
070621	1.55 ± 0.07	...	>116	7.8 ± 0.3	49.1/56 ¹	157^{+381}_{-50}	$2.5^{+1.2}_{-0.5}$	9^{+7}_{-2}	...
070628	1.90 ± 0.09	...	>51	5.1 ± 0.2	50.3/56 ¹	64^{+222}_{-61}	4^{+4}_{-2}	7^{+6}_{-1}	...
070704	1.59 ± 0.08	...	>144	9.6 ± 0.5	48.9/56 ¹	220^{+590}_{-110}	$4.0^{+1.4}_{-1.0}$	14^{+10}_{-4}	...
070714A	...	2.7 ± 0.3	<21	0.17 ± 0.01	56.8/56 ¹	17^{+6}_{-16}	$0.26^{+2.59}_{-0.07}$	$0.30^{+0.90}_{-0.05}$...
070714B	1.3 ± 0.2	...	>72	1.4 ± 0.2	46.0/56 ¹	165^{+499}_{-73}	$0.32^{+0.23}_{-0.10}$	$0.3^{+0.1}_{-0.1}$	0.92 ⁵
070721A	...	$2.8^{+0.6}_{-0.5}$	<28	0.07 ± 0.01	59.1/56 ¹	15^{+10}_{-14}	$0.14^{+1.47}_{-0.07}$	$0.15^{+0.54}_{-0.05}$...
070721B	1.2 ± 0.1	...	>193	7.4 ± 0.6	43.3/56 ¹	410^{+810}_{-200}	8^{+3}_{-2}	30^{+20}_{-10}	3.626 ⁶
070724A	...	2.0 ± 0.4	<72	0.044 ± 0.011	65.1/56 ¹	41^{+101}_{-37}	$0.009^{+0.025}_{-0.004}$	$0.0025^{+0.0031}_{-0.0007}$	0.457 ⁷
070729	1.0 ± 0.3	...	>81	0.24 ± 0.05	52.8/56 ¹	370^{+620}_{-240}	$0.026^{+0.011}_{-0.008}$	$0.3^{+0.5}_{-0.2}$...
070731	1.6 ± 0.3	...	>49	0.26 ± 0.04	38.2/56 ¹	78^{+250}_{-31}	$0.07^{+0.07}_{-0.02}$	$0.23^{+0.24}_{-0.06}$...
070802	1.8 ± 0.3	0.40 ± 0.07	27.8/56 ¹	55^{+267}_{-35}	$0.8^{+1.9}_{-0.4}$	$0.50^{+0.52}_{-0.10}$	2.45 ⁸
070805	1.6 ± 0.2	...	>133	1.1 ± 0.1	50.9/56 ¹	200^{+720}_{-100}	$0.4^{+0.2}_{-0.1}$	$1.5^{+1.4}_{-0.5}$...
070808	1.5 ± 0.2	...	>90	2.3 ± 0.2	56.8/56 ¹	135^{+447}_{-47}	$0.5^{+0.3}_{-0.1}$	$2.3^{+2.9}_{-0.5}$...
070809	1.6 ± 0.2	...	>51	0.14 ± 0.02	44.4/56 ¹	82^{+258}_{-32}	$0.0032^{+0.0034}_{-0.0010}$	$0.0013^{+0.0015}_{-0.0003}$	0.2187 ⁹
070810A	0.7 ± 0.8	...	42 ± 6	$0.57^{+0.05}_{-0.04}$	46.5/55 ²	41 ± 8	$1.7^{+2.1}_{-0.6}$	$0.9^{+0.1}_{-0.1}$	2.17 ¹⁰
070810B	1.0 ± 0.7	...	>43	$0.07^{+0.04}_{-0.03}$	52.8/56 ¹	330^{+920}_{-260}	$0.008^{+0.006}_{-0.004}$	$0.08^{+0.12}_{-0.06}$...
070911	1.4 ± 0.2	...	140^{+230}_{-40}	17.7 ± 1.1	56.8/55 ²	122^{+115}_{-26}	9^{+4}_{-2}	24^{+8}_{-3}	...
070913	1.6 ± 0.3	...	>53	0.33 ± 0.06	47.2/56 ¹	86^{+346}_{-31}	$0.08^{+0.08}_{-0.03}$	$0.29^{+0.36}_{-0.07}$...
070917	1.45 ± 0.06	...	>150	3.5 ± 0.1	45.6/56 ¹	223^{+466}_{-84}	$0.9^{+0.3}_{-0.1}$	$4.5^{+3.7}_{-1.0}$...
070920A	1.7 ± 0.2	...	>51	0.8 ± 0.1	49.0/56 ¹	74^{+317}_{-26}	$0.26^{+0.23}_{-0.09}$	$0.7^{+0.8}_{-0.2}$...
070920B	$-0.1^{+0.9}_{-2.4}$	$2.5^{+0.9}_{-0.4}$	39^{+3}_{-8}	0.82 ± 0.08	43.4/54 ³	44^{+8}_{-6}	$0.4^{+0.2}_{-0.1}$	$1.18^{+0.03}_{-0.32}$...
070923	0.9 ± 0.4	...	>142	$0.12^{+0.03}_{-0.03}$	26.8/27 ¹	430^{+830}_{-280}	$0.012^{+0.006}_{-0.003}$	$0.2^{+0.3}_{-0.1}$...
071001	1.6 ± 0.2	...	>57	1.5 ± 0.2	54.3/56 ¹	82^{+129}_{-29}	$0.4^{+0.3}_{-0.1}$	$1.3^{+0.9}_{-0.3}$...
071003	1.31 ± 0.07	...	>240	16.7 ± 0.7	47.6/56 ¹	410^{+810}_{-190}	11^{+3}_{-2}	18^{+14}_{-6}	1.605 ¹¹
071008	...	2.2 ± 0.3	<52	0.27 ± 0.04	75.1/56 ¹	30^{+17}_{-29}	$0.22^{+0.96}_{-0.08}$	$0.32^{+0.57}_{-0.03}$...
071010A	...	2.1 ± 0.4	<42	0.47 ± 0.11	73.4/56 ¹	37^{+49}_{-35}	$0.4^{+2.5}_{-0.2}$	$0.13^{+0.24}_{-0.02}$	0.98 ¹²
071010B	1.5 ± 0.2	...	57^{+8}_{-6}	5.1 ± 0.2	33.5/55 ²	56 ± 8	6^{+4}_{-2}	$1.8^{+0.4}_{-0.1}$	0.947 ¹³
071011	1.4 ± 0.1	...	>221	5.4 ± 0.4	81.7/56 ¹	370^{+770}_{-200}	$1.2^{+0.4}_{-0.3}$	9^{+7}_{-4}	...
071013	1.6 ± 0.4	...	>45	$0.6^{+0.2}_{-0.1}$	49.6/56 ¹	100^{+675}_{-70}	$0.16^{+0.18}_{-0.07}$	$0.6^{+1.0}_{-0.2}$...
071018	1.6 ± 0.3	...	>83	1.9 ± 0.3	68.7/56 ¹	149^{+615}_{-79}	$0.5^{+0.5}_{-0.2}$	$2.3^{+2.9}_{-0.9}$...
071020	1.05 ± 0.05	...	>224	5.6 ± 0.2	39.8/56 ¹	410^{+650}_{-150}	$2.4^{+0.6}_{-0.3}$	10^{+10}_{-3}	2.145 ¹⁴
071021	1.7 ± 0.2	...	>54	1.8 ± 0.3	70.7/56 ¹	74^{+424}_{-29}	$0.7^{+0.7}_{-0.2}$	$1.7^{+2.0}_{-0.3}$...
071025	1.67 ± 0.06	...	>124	11.0 ± 0.3	43.6/56 ¹	165^{+499}_{-59}	$5.5^{+2.1}_{-0.9}$	15^{+10}_{-3}	...
071028A	0^{+1}_{-2}	...	50^{+70}_{-10}	$0.33^{+0.08}_{-0.05}$	47.0/55 ²	58^{+102}_{-24}	$0.18^{+0.19}_{-0.06}$	$0.5^{+0.3}_{-0.1}$...
071031	...	2.3 ± 0.3	<27	1.1 ± 0.2	49.9/56 ¹	12^{+6}_{-11}	11^{+8}_{-5}	$3.9^{+4.1}_{-0.6}$	2.692 ¹⁵
071101	...	2.2 ± 0.6	<29	$0.08^{+0.03}_{-0.02}$	46.7/56 ¹	30^{+66}_{-29}	$0.06^{+0.26}_{-0.02}$	$0.09^{+0.18}_{-0.01}$...
071112B	0.8 ± 0.5	...	>95	$0.18^{+0.06}_{-0.05}$	60.7/56 ¹	450^{+850}_{-290}	$0.017^{+0.008}_{-0.006}$	$0.3^{+0.4}_{-0.2}$...
071117	1.2 ± 0.3	...	130^{+160}_{-30}	$3.4^{+0.3}_{-0.3}$	52.1/55 ²	128^{+119}_{-35}	$2.6^{+1.8}_{-0.7}$	$1.9^{+0.8}_{-0.3}$	1.331 ¹⁶
071118	1.7 ± 0.4	$0.7^{+0.2}_{-0.1}$	58.2/56 ¹	74^{+582}_{-35}	$0.20^{+0.25}_{-0.07}$	$0.6^{+0.9}_{-0.2}$...
071122	1.6 ± 0.4	...	>57	1.0 ± 0.2	76.2/56 ¹	111^{+325}_{-57}	$0.5^{+0.8}_{-0.2}$	$0.3^{+0.5}_{-0.1}$	1.14 ¹⁷
071129	1.0 ± 0.6	...	70^{+70}_{-10}	$3.0^{+0.5}_{-0.3}$	42.5/55 ²	67^{+44}_{-16}	$1.3^{+1.0}_{-0.4}$	$3.9^{+1.6}_{-0.6}$...
071227	1.1 ± 0.2	...	>92	0.53 ± 0.08	50.5/56 ¹	330^{+580}_{-210}	$0.018^{+0.008}_{-0.006}$	$0.03^{+0.04}_{-0.01}$	0.383 ¹⁸
080123	...	$2.1^{+0.9}_{-0.7}$	<61	$0.18^{+0.08}_{-0.06}$	49.0/56 ¹	45^{+138}_{-44}	$0.09^{+0.70}_{-0.04}$	$0.21^{+0.44}_{-0.07}$...

Continued on Next Page...

TABLE 4 – Continued

GRB	$-\alpha$	$-\beta$	$E_{\text{pk,obs}}^{\text{freq.}}$	$S_{15-350 \text{ keV}}$	$\chi^2/\nu^{(\text{model})}$	$E_{\text{pk,obs}}$	N_{iso} or n_{bol}	E_{iso} or S_{bol}	$z^{(\text{ref})}$
080129	1.2 ± 0.2	...	>77	1.9 ± 0.3	52.7/56 ¹	250_{-150}^{+490}	2_{-1}^{+2}	8_{-4}^{+7}	4.349 ¹⁹
080205	2.0 ± 0.1	2.9 ± 0.2	54.3/56 ¹	50_{-48}^{+35}	$1.8_{-0.4}^{+4.6}$	$3.2_{-0.1}^{+5.0}$...
080207	1.0 ± 0.4	...	100_{-20}^{+130}	$8.7_{-0.8}^{+1.1}$	52.1/55 ²	100_{-21}^{+100}	$2.7_{-0.6}^{+1.9}$	11_{-2}^{+5}	...
080210	1.8 ± 0.1	...	>90	2.7 ± 0.2	43.6/56 ¹	90_{-36}^{+472}	11_{-4}^{+17}	$5.1_{-0.9}^{+4.5}$	2.641 ²⁰
080212	0.4 ± 0.7	...	68_{-9}^{+17}	$3.6_{-0.3}^{+0.4}$	42.3/55 ²	74_{-11}^{+29}	$1.2_{-0.3}^{+0.6}$	$4.6_{-0.5}^{+1.3}$...
080218A	...	2.3 ± 0.4	<46	0.9 ± 0.2	47.0/56 ¹	30_{-28}^{+20}	$0.6_{-0.3}^{+2.5}$	$1.1_{-0.2}^{+1.8}$...
080218B	-1_{-4}^{+3}	...	24_{-17}^{+5}	0.51 ± 0.06	41.0/55 ²	16_{-6}^{+9}	$1.2_{-0.5}^{+1.2}$	$1.3_{-0.3}^{+0.6}$...
080229A	1.87 ± 0.05	...	>84	12.8 ± 0.3	38.1/56 ¹	95_{-31}^{+485}	12_{-3}^{+5}	20_{-3}^{+11}	...
080303	1.6 ± 0.3	...	>97	1.0 ± 0.2	60.1/56 ¹	180_{-110}^{+680}	$0.3_{-0.5}^{+0.2}$	$1.3_{-0.5}^{+1.5}$...
080307	1.7 ± 0.2	...	>69	1.4 ± 0.2	60.8/56 ¹	90_{-40}^{+472}	$0.5_{-0.2}^{+0.3}$	$1.4_{-0.3}^{+1.6}$...
080310	...	2.4 ± 0.2	<29	2.7 ± 0.2	40.9/56 ¹	22_{-20}^{+8}	16_{-6}^{+165}	$5.9_{-1.0}^{+10.5}$	2.4266 ²¹
080319A	1.6 ± 0.1	...	>83	7.2 ± 0.5	51.8/56 ¹	105_{-35}^{+300}	$2.2_{-0.5}^{+2.1}$	8_{-1}^{+7}	...
080319B	1.09 ± 0.02	...	>1382	411 ± 5	17.7/56 ¹	1220_{-540}^{+1590}	75 ± 8	400_{-100}^{+200}	0.937 ²²
080319C	1.0 ± 0.3	...	160_{-50}^{+820}	$5.4_{-0.6}^{+0.8}$	56.2/55 ²	157_{-47}^{+303}	$4.7_{-1.0}^{+3.9}$	6_{-1}^{+5}	1.95 ²³
080319D	-4_{-1}^{+5}	...	34_{-5}^{+9}	$0.22_{-0.03}^{+0.04}$	50.5/55 ²	37_{-32}^{+290}	$0.22_{-0.09}^{+0.48}$	$0.5_{-0.1}^{+0.6}$...
080320	1.6 ± 0.3	...	>63	0.56 ± 0.09	50.9/56 ¹	95_{-39}^{+485}	$0.17_{-0.06}^{+0.14}$	$0.6_{-0.1}^{+0.8}$...
080325	1.7 ± 0.2	...	>86	7.7 ± 0.7	50.7/56 ¹	111_{-41}^{+399}	$2.5_{-0.7}^{+2.6}$	8_{-2}^{+9}	...
080328	1.36 ± 0.05	...	>483	17.9 ± 0.5	34.1/56 ¹	600_{-290}^{+980}	$4.4_{-0.5}^{+0.7}$	50_{-30}^{+10}	...
080330	...	2.4 ± 0.5	<28	0.44 ± 0.09	62.2/56 ¹	20_{-19}^{+6}	$1.5_{-0.6}^{+18.9}$	$0.41_{-0.06}^{+0.94}$	1.51 ²⁴
080409	1.2 ± 0.9	...	40_{-30}^{+10}	$0.52_{-0.05}^{+0.06}$	47.8/55 ²	41 ± 25	$0.4_{-0.1}^{+0.6}$	$0.7_{-0.1}^{+0.6}$...
080411	1.68 ± 0.03	...	>298	43.1 ± 0.4	21.7/56 ¹	410_{-190}^{+810}	54_{-7}^{+10}	23_{-4}^{+9}	1.03 ²⁵
080413A	1.56 ± 0.06	...	>109	5.9 ± 0.2	67.2/56 ¹	149_{-42}^{+370}	12_{-3}^{+9}	9_{-2}^{+6}	2.433 ²⁶
080413B	1.2 ± 0.3	...	69_{-8}^{+15}	3.7 ± 0.2	31.2/55 ²	67_{-8}^{+12}	3_{-1}^{+2}	1.5 ± 0.2	1.10 ²⁷
080426	1.9 ± 0.1	0.54 ± 0.04	45.3/56 ¹	55 ± 54	$0.30_{-0.09}^{+0.71}$	$0.59_{-0.04}^{+0.90}$...
080430	1.74 ± 0.09	...	>113	1.86 ± 0.09	50.7/56 ¹	122_{-49}^{+554}	$1.3_{-0.3}^{+0.9}$	$0.38_{-0.08}^{+0.30}$	0.767 ²⁸
080503	1.9 ± 0.1	2.7 ± 0.2	50.8/56 ¹	50_{-49}^{+18}	$1.7_{-0.4}^{+4.4}$	$2.98_{-0.07}^{+4.73}$...
080506	1.7 ± 0.2	...	>55	2.0 ± 0.3	49.0/56 ¹	67_{-28}^{+402}	$0.8_{-0.3}^{+0.8}$	$1.9_{-0.4}^{+2.2}$...
080515	0_{-1}^{+1}	...	30_{-9}^{+4}	2.2 ± 0.2	40.9/55 ²	26 ± 5	$2.6_{-0.8}^{+1.8}$	$3.9_{-0.5}^{+1.2}$...
080516	1.8 ± 0.3	0.50 ± 0.08	77.0/56 ¹	67_{-38}^{+402}	$0.18_{-0.07}^{+0.23}$	$0.5_{-0.1}^{+0.5}$...
080517	1.5 ± 0.3	...	>56	0.9 ± 0.2	53.3/56 ¹	100_{-41}^{+377}	$0.19_{-0.06}^{+0.18}$	$0.8_{-0.1}^{+1.0}$...
080520	...	$3.4_{-0.6}^{+0.9}$	<19	0.058 ± 0.010	48.2/56 ¹	11_{-10}^{+3}	$0.7_{-0.4}^{+31.1}$	$0.11_{-0.04}^{+1.45}$	1.545 ²⁹
080523	0.9 ± 0.7	...	90_{-20}^{+1330}	$1.0_{-0.1}^{+0.2}$	53.6/55 ²	90_{-26}^{+172}	$0.34_{-0.09}^{+0.25}$	$1.2_{-0.2}^{+0.9}$...
080602	1.5 ± 0.1	...	>80	6.1 ± 0.5	60.8/56 ¹	116_{-44}^{+252}	$1.3_{-0.3}^{+1.0}$	6_{-1}^{+5}	...
080603B	1.2 ± 0.3	...	70_{-10}^{+30}	$2.9_{-0.2}^{+0.2}$	65.4/55 ²	70_{-12}^{+17}	9_{-4}^{+9}	6 ± 1	2.69 ³⁰
080604	1.7 ± 0.2	...	>56	1.5 ± 0.2	47.9/56 ¹	74_{-29}^{+424}	$1.4_{-0.6}^{+2.4}$	$0.7_{-0.1}^{+0.8}$	1.416 ³¹
080607	1.17 ± 0.04	...	>860	51 ± 1	41.4/56 ¹	900_{-460}^{+1170}	52_{-7}^{+8}	280_{-90}^{+130}	3.036 ³²
080605	1.1 ± 0.2	...	230_{-60}^{+250}	22 ± 1	30.7/55 ²	223_{-60}^{+207}	16_{-4}^{+6}	21_{-4}^{+9}	1.6398 ³³
080613B	1.36 ± 0.06	...	>456	10.6 ± 0.3	51.2/56 ¹	550_{-240}^{+1160}	$2.7_{-0.3}^{+0.4}$	22_{-8}^{+16}	...
080623	1.4 ± 0.2	...	>93	2.0 ± 0.2	53.0/56 ¹	182_{-82}^{+528}	$0.39_{-0.09}^{+0.21}$	$2.2_{-0.7}^{+2.7}$...
080701	...	2.0 ± 0.1	<52	0.92 ± 0.07	53.2/56 ¹	43_{-39}^{+16}	$0.5_{-0.2}^{+1.1}$	$0.96_{-0.10}^{+1.55}$...
080702A	1.3 ± 0.4	...	>57	$0.08_{-0.02}^{+0.02}$	45.6/56 ¹	200_{-140}^{+560}	$0.013_{-0.004}^{+0.012}$	$0.09_{-0.04}^{+0.10}$...
080703	1.7 ± 0.3	...	>44	0.35 ± 0.06	61.2/56 ¹	64_{-27}^{+172}	$0.11_{-0.04}^{+0.11}$	$0.31_{-0.06}^{+0.28}$...
080707	1.7 ± 0.2	...	>58	1.0 ± 0.1	58.2/56 ¹	74_{-32}^{+317}	$0.8_{-0.3}^{+1.2}$	$0.34_{-0.05}^{+0.41}$	1.23 ³⁴
080710	1.3 ± 0.2	...	>81	3.2 ± 0.5	49.6/56 ¹	300_{-200}^{+550}	$0.6_{-0.2}^{+0.4}$	$0.8_{-0.4}^{+0.8}$	0.845 ³⁵
080714	1.44 ± 0.09	...	>101	4.8 ± 0.3	64.4/56 ¹	149_{-42}^{+370}	$1.0_{-0.2}^{+0.6}$	5_{-1}^{+4}	...
080721	0.95 ± 0.09	...	>283	34 ± 1	57.2/56 ¹	600_{-290}^{+980}	15_{-3}^{+4}	110_{-50}^{+110}	2.602 ³⁶
080723A	-5 ± 3	$2.2_{-0.2}^{+0.5}$	35 ± 5	0.52 ± 0.09	57.8/54 ³	74_{-32}^{+121}	$0.17_{-0.05}^{+0.15}$	$0.6_{-0.1}^{+0.5}$...
080725	1.5 ± 0.1	...	>130	6.6 ± 0.4	50.5/56 ¹	182_{-74}^{+528}	$1.8_{-0.4}^{+0.9}$	8_{-2}^{+8}	...
080727A	1.2 ± 0.4	...	>61	$0.28_{-0.07}^{+0.09}$	66.8/56 ¹	220_{-150}^{+590}	$0.04_{-0.01}^{+0.04}$	$0.3_{-0.2}^{+0.5}$...
080727B	1.05 ± 0.07	...	>170	8.1 ± 0.4	50.2/56 ¹	370_{-130}^{+770}	$0.9_{-0.1}^{+0.2}$	12_{-1}^{+14}	...
080727C	0.9 ± 0.2	...	190_{-50}^{+280}	$8.8_{-0.8}^{+0.9}$	73.3/55 ²	192_{-57}^{+277}	$1.7_{-0.2}^{+0.5}$	11_{-2}^{+9}	...
080802	1.7 ± 0.2	...	>46	2.1 ± 0.3	56.5/56 ¹	61_{-20}^{+106}	$0.7_{-0.2}^{+0.7}$	$1.8_{-0.3}^{+1.2}$...
080804	1.0 ± 0.1	...	>165	9.0 ± 0.6	41.2/56 ¹	410_{-200}^{+650}	$3.8_{-0.8}^{+1.3}$	16_{-7}^{+17}	2.200 ³⁷
080805	1.54 ± 0.09	...	>151	4.5 ± 0.2	46.1/56 ¹	300_{-190}^{+550}	6_{-2}^{+3}	4_{-2}^{+2}	1.505 ³⁸
080810	1.3 ± 0.1	...	>174	9.7 ± 0.7	40.9/56 ¹	370_{-220}^{+620}	15_{-5}^{+8}	30_{-20}^{+30}	3.35 ³⁹
080822B	-2_{-3}^{+4}	...	<45	$0.13_{-0.03}^{+0.03}$	61.5/55 ²	27_{-26}^{+49}	$0.15_{-0.08}^{+0.78}$	$0.25_{-0.07}^{+0.47}$...

Continued on Next Page...

TABLE 4 – Continued

GRB	$-\alpha$	$-\beta$	$E_{\text{pk,obs}}^{\text{freq.}}$	$S_{15-350 \text{ keV}}$	$\chi^2/\nu^{(\text{model})}$	$E_{\text{pk,obs}}$	N_{iso} or n_{bol}	E_{iso} or S_{bol}	$z^{(\text{ref})}$
080903	0.9 ± 0.6	...	63^{+29}_{-10}	$1.8^{+0.2}_{-0.2}$	60.0/55 ²	64^{+25}_{-11}	$0.8^{+0.5}_{-0.2}$	$2.3^{+0.6}_{-0.3}$...
080905A	0.9 ± 0.3	...	>119	0.40 ± 0.07	52.9/56 ¹	450^{+850}_{-250}	$0.034^{+0.014}_{-0.006}$	$0.7^{+1.1}_{-0.4}$...
080905B	1.7 ± 0.2	...	>65	2.8 ± 0.3	45.8/56 ¹	82^{+258}_{-21}	5^{+9}_{-2}	$3.4^{+3.1}_{-0.6}$	2.374 ⁴⁰
080906	1.58 ± 0.09	...	>83	6.4 ± 0.3	32.9/56 ¹	105^{+236}_{-31}	$1.9^{+1.4}_{-0.3}$	6^{+5}_{-1}	...
080913	0.4 ± 0.9	...	100^{+140}_{-20}	$0.8^{+0.2}_{-0.1}$	64.3/55 ²	135^{+276}_{-47}	$2.1^{+0.8}_{-0.8}$	7^{+1}_{-1}	6.7 ⁴¹
080915A	1.7 ± 0.3	0.33 ± 0.07	36.8/56 ¹	64^{+391}_{-36}	$0.10^{+0.13}_{-0.04}$	$0.29^{+0.40}_{-0.06}$...
080915B	1.96 ± 0.08	...	>37	1.46 ± 0.06	47.2/56 ¹	50 ± 38	$0.9^{+0.9}_{-0.4}$	$2.7^{+0.9}_{-1.1}$...
080916A	1.1 ± 0.2	...	110^{+50}_{-20}	5.6 ± 0.4	51.8/55 ²	105^{+43}_{-17}	$1.5^{+0.7}_{-0.3}$	$0.81^{+0.21}_{-0.09}$	0.689 ⁴²
080916B	1.5 ± 0.2	...	>53	1.1 ± 0.2	56.7/56 ¹	100^{+377}_{-37}	$0.22^{+0.20}_{-0.06}$	$1.0^{+1.4}_{-0.3}$...
080919	1.3 ± 0.3	...	>125	0.19 ± 0.04	52.9/56 ¹	370^{+770}_{-240}	$0.04^{+0.02}_{-0.01}$	$0.3^{+0.3}_{-0.2}$...
080928	1.7 ± 0.1	...	>63	4.0 ± 0.3	43.3/56 ¹	74^{+243}_{-26}	6^{+10}_{-2}	$2.8^{+2.4}_{-0.5}$	1.692 ⁴³
081007	$1.4^{+0.6}_{-1.0}$...	<35	$0.59^{+0.06}_{-0.05}$	59.4/55 ²	27^{+11}_{-16}	$0.4^{+0.8}_{-0.2}$	$0.07^{+0.05}_{-0.01}$	0.5295 ⁴⁴
081008	1.3 ± 0.3	...	110^{+430}_{-30}	$5.6^{+0.7}_{-0.5}$	53.5/55 ²	90^{+113}_{-21}	9^{+12}_{-3}	6^{+3}_{-1}	1.9685 ⁴⁵
081011	1.6 ± 0.3	...	>44	0.39 ± 0.08	66.0/56 ¹	82^{+336}_{-40}	$0.09^{+0.09}_{-0.03}$	$0.34^{+0.48}_{-0.09}$...
081012	0.9 ± 0.2	...	>110	3.5 ± 0.5	64.5/56 ¹	450^{+250}_{-10}	$0.31^{+0.11}_{-0.06}$	6^{+10}_{-4}	...
081016B	0.5 ± 0.4	...	>93	$0.27^{+0.08}_{-0.06}$	43.6/56 ¹	550^{+930}_{-310}	$0.016^{+0.007}_{-0.004}$	$0.4^{+0.9}_{-0.3}$...
081017	1.7 ± 0.3	...	>48	2.1 ± 0.3	37.2/56 ¹	74^{+317}_{-32}	$0.7^{+0.8}_{-0.2}$	$2.0^{+2.1}_{-0.5}$...
081022	0.9 ± 0.6	...	80^{+70}_{-20}	$2.7^{+0.4}_{-0.3}$	45.3/55 ²	78^{+58}_{-17}	$1.0^{+0.6}_{-0.3}$	$7.4^{+0.4}_{-3.8}$...
081024A	1.2 ± 0.2	...	>102	0.26 ± 0.04	71.7/56 ¹	330^{+580}_{-210}	$0.04^{+0.02}_{-0.01}$	$0.4^{+0.5}_{-0.2}$...
081028	1.3 ± 0.4	...	70^{+70}_{-10}	$4.3^{+0.5}_{-0.4}$	45.2/55 ²	67^{+31}_{-4}	18^{+25}_{-5}	11^{+3}_{-3}	3.038 ⁴⁶
081029	1.4 ± 0.2	...	>129	3.3 ± 0.4	52.6/56 ¹	300^{+550}_{-200}	8^{+7}_{-4}	15^{+9}_{-7}	3.8479 ⁴⁷
081101	-1^{+1}_{-2}	...	80^{+40}_{-10}	$0.08^{+0.02}_{-0.01}$	24.6/26 ²	165^{+499}_{-59}	$0.020^{+0.010}_{-0.005}$	$0.15^{+0.26}_{-0.05}$...
081102	1.7 ± 0.1	...	>60	3.8 ± 0.3	49.7/56 ¹	78^{+125}_{-22}	$1.1^{+1.0}_{-0.3}$	$3.4^{+2.2}_{-0.6}$...
081104	1.9 ± 0.1	...	>48	2.7 ± 0.2	52.3/56 ¹	61^{+58}_{-20}	$1.1^{+1.2}_{-0.3}$	$2.7^{+1.3}_{-0.5}$...
081109A	1.3 ± 0.3	...	120^{+490}_{-40}	$4.3^{+0.5}_{-0.4}$	40.1/55 ²	105^{+153}_{-25}	$1.6^{+1.0}_{-0.3}$	$5.3^{+3.0}_{-0.8}$...
081109B	...	$2.1^{+0.7}_{-0.6}$	<81	$0.30^{+0.12}_{-0.09}$	60.4/56 ¹	33^{+56}_{-32}	$0.18^{+0.81}_{-0.09}$	$0.35^{+0.61}_{-0.10}$...
081118	...	2.1 ± 0.2	<52	1.6 ± 0.1	54.8/56 ¹	37^{+12}_{-35}	7^{+43}_{-3}	$2.8^{+4.4}_{-0.4}$	2.58 ⁴⁸
081121	0.5 ± 0.6	...	130^{+160}_{-30}	$7.9^{+1.2}_{-0.9}$	43.1/55 ²	182^{+332}_{-60}	6^{+5}_{-1}	16^{+15}_{-4}	2.512 ⁴⁹
081126	0.9 ± 0.3	...	220^{+3140}_{-80}	$6.0^{+0.8}_{-0.6}$	41.0/55 ²	250^{+400}_{-100}	$1.1^{+0.3}_{-0.2}$	9^{+9}_{-2}	...
081127	2.0 ± 0.4	0.6 ± 0.1	38.4/56 ¹	50^{+61}_{-49}	$0.35^{+1.69}_{-0.09}$	$0.715^{+1.267}_{-0.006}$...
081128	0.9 ± 0.6	...	47^{+6}_{-5}	$2.5^{+0.2}_{-0.1}$	45.0/55 ²	46 ± 6	$1.5^{+0.8}_{-0.4}$	$3.5^{+0.7}_{-0.4}$...
081203A	1.44 ± 0.06	...	>128	13.6 ± 0.5	57.5/56 ¹	201^{+440}_{-75}	16^{+9}_{-4}	17^{+13}_{-4}	2.1 ⁵⁰
081210	1.4 ± 0.1	...	>116	3.7 ± 0.4	54.0/56 ¹	220^{+590}_{-110}	$0.8^{+0.4}_{-0.2}$	5^{+5}_{-2}	...
081211A	...	2.0 ± 0.5	<33	$0.19^{+0.06}_{-0.05}$	43.6/56 ¹	37^{+75}_{-36}	$0.11^{+0.50}_{-0.05}$	$0.21^{+0.38}_{-0.04}$...
081221	1.1 ± 0.1	...	83^{+8}_{-5}	22.4 ± 0.7	31.3/55 ²	81^{+7}_{-4}	9^{+2}_{-1}	28^{+3}_{-3}	...
081222	1.0 ± 0.2	...	140^{+50}_{-20}	7.3 ± 0.4	47.5/55 ²	135^{+52}_{-23}	10^{+5}_{-2}	15^{+3}_{-2}	2.77 ⁵¹
081226A	1.3 ± 0.3	...	>73	0.21 ± 0.05	60.9/56 ¹	250^{+620}_{-150}	$0.03^{+0.03}_{-0.01}$	$0.3^{+0.3}_{-0.1}$...
081228	2.0 ± 0.3	0.14 ± 0.03	44.3/56 ¹	39^{+78}_{-34}	$0.07^{+0.14}_{-0.03}$	$0.15^{+0.20}_{-0.03}$...
081230	1.0 ± 0.8	...	52^{+23}_{-9}	$0.84^{+0.11}_{-0.08}$	43.4/55 ²	52^{+19}_{-14}	$0.5^{+0.3}_{-0.1}$	$1.2^{+0.3}_{-0.2}$...
090102	1.36 ± 0.10	...	>182	14.2 ± 0.8	55.9/56 ¹	370^{+520}_{-220}	10 ± 3	14^{+10}_{-5}	1.547 ⁵²
090107A	$-4.8^{+6.0}_{-0.2}$	$2.3^{+1.0}_{-0.3}$	30 ± 4	$0.29^{+0.08}_{-0.06}$	39.2/54 ³	50^{+252}_{-29}	$0.15^{+0.19}_{-0.05}$	$0.4^{+0.3}_{-0.1}$...
090111	...	2.4 ± 0.2	<28	0.80 ± 0.07	59.7/56 ¹	22^{+14}_{-21}	$0.9^{+4.9}_{-0.2}$	$1.23^{+2.13}_{-0.05}$...
090113	1.5 ± 0.1	...	>94	1.32 ± 0.08	41.2/56 ¹	128^{+434}_{-40}	$0.35^{+0.22}_{-0.07}$	$1.3^{+1.3}_{-0.3}$...
090123	1.6 ± 0.1	...	>92	4.7 ± 0.4	53.2/56 ¹	116^{+410}_{-39}	$1.4^{+1.1}_{-0.4}$	5^{+5}_{-1}	...
090129	1.4 ± 0.3	...	70^{+30}_{-10}	$2.5^{+0.2}_{-0.2}$	66.3/55 ²	65^{+16}_{-12}	$1.5^{+0.8}_{-0.4}$	$3.4^{+0.5}_{-0.4}$...
090201	0.8 ± 0.2	...	100^{+20}_{-10}	40 ± 1	46.5/55 ²	103^{+17}_{-13}	10^{+2}_{-2}	47 ± 5	...
090205	1^{+1}_{-2}	...	<45	$0.19^{+0.03}_{-0.02}$	51.8/55 ²	33 ± 31	$1.9^{+10.2}_{-0.9}$	$1.2^{+1.6}_{-0.2}$	4.6497 ⁵³
090301	0.9 ± 0.1	...	240^{+140}_{-60}	42 ± 2	34.7/55 ²	246^{+131}_{-60}	$7.0^{+0.9}_{-0.7}$	110 ± 30	...
090305	1.1 ± 0.3	...	>72	0.22 ± 0.05	50.9/56 ¹	270^{+520}_{-170}	$0.027^{+0.017}_{-0.008}$	$0.3^{+0.4}_{-0.1}$...
090307	-5 ± 1	$2.01^{+1.65}_{-0.01}$	51^{+13}_{-8}	0.32 ± 0.05	59.6/54 ³	330^{+730}_{-230}	$0.07^{+0.04}_{-0.02}$	$0.8^{+1.1}_{-0.5}$...
090308	$1.9^{+0.6}_{-0.5}$	$0.6^{+0.2}_{-0.2}$	67.0/56 ¹	47^{+332}_{-45}	$0.3^{+1.1}_{-0.1}$	$0.7^{+1.0}_{-0.2}$...
090309	1.3 ± 0.4	...	>76	$0.27^{+0.07}_{-0.06}$	57.8/56 ¹	300^{+690}_{-200}	$0.05^{+0.04}_{-0.01}$	$0.4^{+0.4}_{-0.2}$...
090313	1.9 ± 0.3	2.2 ± 0.4	51.9/56 ¹	55^{+202}_{-51}	7^{+26}_{-4}	$4.6^{+7.0}_{-0.5}$	3.375 ⁵⁴
090401A	1.4 ± 0.2	...	130^{+160}_{-30}	14.7 ± 1.1	57.4/55 ²	116^{+92}_{-28}	6^{+3}_{-1}	19^{+7}_{-3}	...
090401B	1.24 ± 0.05	...	>255	21.4 ± 0.6	55.1/56 ¹	450^{+510}_{-210}	$3.8^{+0.7}_{-0.4}$	40^{+30}_{-10}	...
090404	$1.8^{+0.2}_{-0.4}$...	<33	$3.1^{+0.2}_{-0.2}$	49.8/55 ²	31^{+4}_{-30}	$3.8^{+12.6}_{-0.8}$	$5.01^{+7.40}_{-0.02}$...

Continued on Next Page...

TABLE 4 – Continued

GRB	$-\alpha$	$-\beta$	$E_{\text{pk,obs}}^{\text{freq.}}$	$S_{15-350 \text{ keV}}$	$\chi^2/\nu^{(\text{model})}$	$E_{\text{pk,obs}}$	N_{iso} or n_{bol}	E_{iso} or S_{bol}	$z^{(\text{ref})}$
090407	1.5 ± 0.4	...	>49	$1.1^{+0.3}_{-0.2}$	50.9/56 ¹	100^{+498}_{-50}	$0.23^{+0.23}_{-0.08}$	$1.0^{+1.8}_{-0.3}$...
090408	...	$2.9^{+1.8}_{-1.0}$	<25	$0.09^{+0.04}_{-0.03}$	40.0/56 ¹	11^{+17}_{-10}	$0.2^{+4.5}_{-0.2}$	$0.2^{+0.5}_{-0.1}$...
090410	0.8 ± 0.2	...	170^{+120}_{-40}	9.2 ± 0.9	49.7/55 ²	192^{+187}_{-45}	$1.5^{+0.4}_{-0.2}$	12^{+7}_{-3}	...
090417A	-1^{+2}_{-4}	...	70^{+150}_{-20}	$0.046^{+0.013}_{-0.008}$	17.0/11 ²	111^{+399}_{-56}	$0.016^{+0.013}_{-0.006}$	$0.07^{+0.12}_{-0.02}$...
090417B	1.7 ± 0.1	...	>101	3.1 ± 0.3	52.6/56 ¹	111^{+708}_{-41}	$1.6^{+0.3}_{-0.4}$	$3.9^{+4.0}_{-0.8}$...
090418	1.39 ± 0.07	...	>172	8.7 ± 0.4	40.4/56 ¹	330^{+580}_{-180}	7^{+2}_{-3}	9^{+6}_{-3}	1.608 ⁵⁵
090419	1.3 ± 0.2	...	>91	4.7 ± 0.5	53.6/56 ¹	182^{+528}_{-82}	$0.9^{+0.5}_{-0.2}$	5^{+7}_{-2}	...
090422	1.6 ± 0.4	...	>41	$0.6^{+0.2}_{-0.1}$	56.8/56 ¹	90^{+642}_{-53}	$0.16^{+0.18}_{-0.06}$	$0.6^{+0.9}_{-0.2}$...
090423	0.7 ± 0.6	...	51^{+9}_{-6}	$0.67^{+0.06}_{-0.05}$	55.3/55 ²	52^{+10}_{-8}	4^{+6}_{-8}	8^{+2}_{-1}	8.3 ⁵⁶
090424	1.1 ± 0.2	...	130^{+40}_{-20}	28 ± 1	33.9/55 ²	128^{+11}_{-22}	$4.3^{+1.1}_{-0.7}$	2.6 ± 0.4	0.544 ⁵⁷
090426	...	2.0 ± 0.3	<212	0.25 ± 0.04	54.5/56 ¹	45^{+57}_{-43}	$0.9^{+7.6}_{-0.3}$	$0.42^{+0.72}_{-0.04}$	2.609 ⁵⁸
090429A	0.7 ± 0.7	...	90^{+210}_{-20}	$0.8^{+0.2}_{-0.1}$	48.7/55 ²	111^{+244}_{-33}	$0.23^{+0.16}_{-0.05}$	$1.1^{+1.1}_{-0.2}$...
090429B	0.7 ± 0.9	...	46^{+11}_{-7}	$0.34^{+0.04}_{-0.03}$	55.8/55 ²	47^{+12}_{-9}	$0.21^{+0.14}_{-0.06}$	$0.49^{+0.14}_{-0.07}$...
090509	1.9 ± 0.3	3.8 ± 0.5	51.9/56 ¹	55^{+202}_{-51}	$1.6^{+3.4}_{-0.7}$	$3.8^{+5.4}_{-0.6}$...
090510	1.0 ± 0.2	...	>97	1.1 ± 0.2	52.0/56 ¹	370^{+920}_{-220}	$0.13^{+0.05}_{-0.03}$	$0.3^{+0.5}_{-0.2}$	0.903 ⁵⁹
090515	0^{+1}_{-2}	...	90^{+2180}_{-30}	$0.035^{+0.014}_{-0.007}$	13.6/11 ²	182^{+528}_{-99}	$0.009^{+0.006}_{-0.003}$	$0.06^{+0.12}_{-0.03}$...
090516	1.6 ± 0.1	...	>101	15 ± 1	69.7/56 ¹	135^{+584}_{-47}	50^{+70}_{-20}	50^{+50}_{-10}	4.109 ⁶⁰
090518	1.5 ± 0.2	...	>68	1.0 ± 0.2	46.9/56 ¹	135^{+447}_{-70}	$0.23^{+0.18}_{-0.07}$	$1.0^{+1.5}_{-0.4}$...
090519	1.0 ± 0.2	...	>129	3.3 ± 0.5	48.5/56 ¹	410^{+810}_{-220}	$2.3^{+1.2}_{-0.6}$	15^{+13}_{-8}	3.85 ⁶¹
090529	1^{+1}_{-1}	...	40^{+20}_{-10}	$1.1^{+0.2}_{-0.1}$	43.1/55 ²	43^{+31}_{-17}	5^{+7}_{-2}	$2.5^{+1.4}_{-0.6}$	2.625 ⁶²
090530	1.6 ± 0.2	...	>63	1.8 ± 0.2	45.6/56 ¹	90^{+215}_{-33}	$0.5^{+0.4}_{-0.1}$	$1.7^{+1.6}_{-0.3}$...
090531A	0.7 ± 0.6	...	64^{+24}_{-10}	$1.6^{+0.2}_{-0.1}$	78.4/55 ²	67^{+26}_{-13}	$0.6^{+0.4}_{-0.2}$	$2.1^{+0.5}_{-0.3}$...
090531B	1.6 ± 0.2	...	>112	1.1 ± 0.2	45.8/56 ¹	165^{+648}_{-81}	$0.4^{+0.3}_{-0.1}$	$1.4^{+1.5}_{-0.4}$...
090607	1.2 ± 0.3	...	>84	0.26 ± 0.05	45.5/56 ¹	300^{+550}_{-200}	$0.036^{+0.023}_{-0.010}$	$0.3^{+0.5}_{-0.2}$...
090618	1.29 ± 0.08	...	140^{+20}_{-10}	148 ± 2	14.4/55 ²	138^{+21}_{-12}	31 ± 4	15 ± 1	0.54 ⁶³
090621B	0.8 ± 0.3	...	>128	0.22 ± 0.04	22.4/27 ¹	500^{+890}_{-280}	$0.018^{+0.006}_{-0.004}$	$0.4^{+0.7}_{-0.2}$...
090628	1.4 ± 0.2	...	>103	1.4 ± 0.2	56.2/56 ¹	200^{+560}_{-100}	$0.32^{+0.18}_{-0.10}$	$1.7^{+1.8}_{-0.7}$...
090708	0^{+1}_{-1}	...	60^{+20}_{-10}	$0.63^{+0.10}_{-0.07}$	58.2/55 ²	61^{+41}_{-20}	$0.3^{+0.3}_{-0.1}$	$0.9^{+0.6}_{-0.2}$...
090709A	1.1 ± 0.1	...	300^{+500}_{-100}	46 ± 2	38.7/55 ²	300^{+365}_{-85}	$8.6^{+1.3}_{-1.0}$	120^{+20}_{-30}	...
090709B	0.4 ± 1.1	...	70^{+50}_{-10}	$1.5^{+0.3}_{-0.2}$	54.7/55 ²	82^{+106}_{-23}	$0.6^{+0.5}_{-0.2}$	$2.1^{+1.7}_{-0.4}$...
090712	1.4 ± 0.1	...	>107	6.9 ± 0.5	52.6/56 ¹	182^{+528}_{-67}	$1.3^{+0.7}_{-0.2}$	7^{+9}_{-2}	...
090715A	1.1 ± 0.2	...	>110	0.9 ± 0.1	53.4/56 ¹	370^{+770}_{-200}	$0.09^{+0.05}_{-0.02}$	$1.3^{+2.2}_{-0.6}$...
090715B	1.61 ± 0.07	...	>130	9.0 ± 0.4	54.8/56 ¹	182^{+528}_{-82}	37^{+19}_{-8}	24^{+15}_{-5}	3.0 ⁶⁴
090726	$1.2^{+0.8}_{-1.3}$...	<37	$0.65^{+0.08}_{-0.06}$	51.8/55 ²	27^{+13}_{-22}	5^{+21}_{-3}	$1.8^{+2.1}_{-0.4}$	2.71 ⁶⁵
090727	1.3 ± 0.3	...	>68	2.6 ± 0.5	63.6/56 ¹	165^{+499}_{-48}	$0.5^{+0.3}_{-0.2}$	$2.6^{+4.1}_{-1.0}$...
090728	1.8 ± 0.2	1.4 ± 0.2	51.6/56 ¹	61^{+381}_{-37}	$0.6^{+0.6}_{-0.2}$	$1.4^{+1.7}_{-0.2}$...
090807	$1.4^{+0.6}_{-0.9}$...	<34	$1.9^{+0.2}_{-0.2}$	61.8/55 ²	27^{+9}_{-18}	$2.1^{+3.5}_{-0.7}$	$3.5^{+2.2}_{-0.9}$...
090809	1.7 ± 0.6	$0.9^{+0.3}_{-0.3}$	41.3/56 ¹	74^{+826}_{-68}	2^{+7}_{-1}	$1.4^{+2.4}_{-0.4}$	2.737 ⁶⁶
090812	1.30 ± 0.06	...	>144	11.6 ± 0.5	49.6/56 ¹	246^{+493}_{-94}	11^{+5}_{-2}	19^{+17}_{-3}	2.452 ⁶⁷
090813	1.6 ± 0.1	...	>132	2.4 ± 0.2	56.9/56 ¹	165^{+648}_{-73}	$1.1^{+0.5}_{-0.2}$	$3.3^{+3.2}_{-0.8}$...

Notes: The model in column 6 refers to a powerlaw (1), a powerlaw times exponential (2), a GRBM (3). If a redshift is known, it is given in the last table column and we present isotropic equivalent energy and photon fluences, E_{iso} and N_{iso} , respectively, in columns 8 and 9. Otherwise, we report approximate bolometric fluences measured in the observer frame $1 - 10^4$ keV band in those columns. Additional details can be found in

Paper I. Redshift References: ¹Perley et al. (2009b), ²Fox & Cucchiara (2007), ³Thoene et al. (2007a), ⁴Centko et al. (2007a), ⁵Graham et al. (2007), ⁶Malesani et al. (2007), ⁷Cucchiara et al. (2007a), ⁸Prochaska et al. (2007a), ⁹Perley et al. (2008b), ¹⁰Thoene et al. (2007b), ¹¹Perley et al. (2007), ¹²Prochaska et al. (2007b), ¹³Centko et al. (2007b), ¹⁴Jakobsson et al. (2007a), ¹⁵Ledoux et al. (2007), ¹⁶Jakobsson et al. (2007b), ¹⁷Cucchiara et al. (2007b), ¹⁸D'Avanzo et al. (2007), ¹⁹Greiner et al. (2008), ²⁰Jakobsson et al. (2008a), ²¹Prochaska et al. (2008a), ²²Vreeswijk et al. (2008a), ²³Wiersema et al. (2008b), ²⁴Malesani et al. (2008), ²⁵Thoene et al. (2008a), ²⁶Thoene et al. (2008b), ²⁷Vreeswijk et al. (2008b), ²⁸Cucchiara & Fox (2008), ²⁹Jakobsson et al. (2008b), ³⁰Fynbo et al. (2008a), ³¹Wiersema et al. (2008a), ³²Prochaska et al. (2008b), ³³Jakobsson et al. (2008c), ³⁴Fynbo et al. (2008b), ³⁵Perley et al. (2008a), ³⁶D'Avanzo et al. (2008a), ³⁷Cucchiara et al. (2008a), ³⁸Jakobsson et al. (2008d), ³⁹Prochaska et al. (2008c), ⁴⁰Vreeswijk et al. (2008c), ⁴¹Fynbo et al. (2008c), ⁴²Fynbo et al. (2008d), ⁴³Vreeswijk et al. (2008d), ⁴⁴Berger et al. (2008a), ⁴⁵D'Avanzo et al. (2008b), ⁴⁶Berger et al. (2008b), ⁴⁷D'Elia et al. (2008a), ⁴⁸D'Elia et al. (2008b), ⁴⁹Berger & Rauch (2008), ⁵⁰Landsman et al. (2008), ⁵¹Cucchiara et al. (2008b), ⁵²de Ugarto Postigo et al. (2009c), ⁵³Fugazza et al. (2009), ⁵⁴Chornock et al. (2009a), ⁵⁵Chornock et al. (2009b), ⁵⁶Tanvir et al. (2009), ⁵⁷Chornock et al. (2009c), ⁵⁸Levesque et al. (2009), ⁵⁹Rau et al. (2009), ⁶⁰de Ugarto Postigo et al. (2009a), ⁶¹Thoene et al. (2009), ⁶²Malesani et al. (2009a), ⁶³Centko et al. (2009b), ⁶⁴Wiersema et al. (2009), ⁶⁵Fatkhullin et al. (2009), ⁶⁶Malesani et al. (2009b), ⁶⁷de Ugarto Postigo et al. (2009b),